الجمهورية الجـزائـرية الديمقراطيـة الشـعبيـــة

وزارة التعليم العـــالي والبـحث العلمـي

PEOPLE 'S DEMOCRATIC REPUBLIC OF ALGERIA

MINISTERY OF HIGH EDUCATION AND SCIENTIFIC RESEARCH

جـــامعة سـعد د حلـب البـليـــدة1

UNIVERSITY OF SAAD DAHLEB BLIDA 1

كلية العلوم – دائرة الفيزياء

Faculty of science
Department of Physics

MASTER DIPLOMA THESIS

In physics

Option: NanoPhysics

THEME

Elaboration and characterization techniques of silicon nitride

Submitted by: **Bouras** Ibtissem

Bensalem Samir

Defended on 06/10/2019 in front of the jury composed of:

Dr. H. Tahi	DR	CDTA	President
Dr. N. Ouarab	MRB	CRTSE	Supervisor
Dr. A. Hassein-Bey	MCB	USDB1	Co-Supervisor
Dr. S. Lafane	MRB	CDTA	Examiner

Blida 1-2018/2019

<u>Acknowledgement</u>

<u>Acknowledgement</u>

I would like to thank my memory promoter N.OUARAB research master at CRTSE Algiers, for his availability and his wise advice, who contributed a lot to this work. I also thank the entire team and professional stakeholders of CRTSE who participated in securing part of my internship. I also wish to express my gratitude to Mlle. Bouras Ibtissem for her efforts during this internship, Mr. Hassein Bey, who has taught me a lot in the world of Nanophysics and all my teachers, parents for all their constant support and encouragement.

Samir BENSALEM

Abstract

Abstract

Silicon nitride is a dielectric material in which optical and mechanical properties strongly depend on the method and the deposition conditions. In the photovoltaic field, the most widespread technique for developing thin films of silicon nitride is Chemical Vapor Deposition (CVD), and more particularly plasma-enhanced CVD (PECVD). The elaboration conditions due to the temperature, pressure, gas ratio, and plasma frequency, therefore, are controlled in a highly reproducible manner, providing an approach to synthesize the Si_3N_4 and to understand the behavior of phase separation of Si_3N_4 material. However, the heating process in a Tempress classical furnace at 1150°C assists in the crystallographic formation of the alpha phase. But seeing the limitation, the beta phase can exist with a low density requiring a high-annealing temperature; this seems to have an important effect on surface morphology, structural and optical properties of silicon nitride films.

Keywords: Si_3N_4, thin film, chemical vapor deposition, characterizations, PECVD.

Résumé

Le nitrure de silicium est un matériau diélectrique dont les propriétés optiques et mécaniques dépendent fortement de la méthode et des conditions de dépôt. Dans le domaine photovoltaïque, la technique la plus répondue pour le développement de couches minces de nitrure de silicium est le dépôt chimique en phase vapeur (CVD), et plus particulièrement le dépôt chimique en phase vapeur (PECVD). Les conditions d'élaboration dues à la température, à la pression, au ratio de gaz et à la fréquence du plasma sont donc contrôlées d'une manière hautement reproductible, ce qui permet de synthétiser le Si_3N_4 et de comprendre la formation de ses phases cristallographiques. Cependant, le processus de chauffage dans un four classique Tempress à 1150°C aide à la formation cristallographique de la phase alpha. Mais vu la limitation, la phase bêta peut exister avec une faible densité nécessitant une température de recuit élevée, ce qui semble avoir un effet important sur la morphologie de surface, les propriétés structurelles et optiques des films de nitrure de silicium.

Mots clés: Si_3N_4, film mince, dépôt chimique en phase vapeur, caractérisations, PECVD.

Abbreviations

MEMS	Micro Electro Mechanical systems
TFT	Thin Film Transistors
MNOS	Metal Nitride Oxide Silicon
CVD	Chemical Vapor Deposition
PECVD	Plasma Enhanced Chemical Vapor Deposition
RF	Radio Frequency
GIXRD	Grazing Incidence X-Ray Diffraction
FE-SEM	Field Effect Scanning Electron Microscopy
AFM	Atomic Force Microscopy
QSSPC	Quasi Steady State Photo-Conductance
UV-VIS-IR	Ultraviolet-Visible-Infrarouge
ARC	Anti Reflective Coating
APCVD	Atmospheric Pressure Chemical Vapor Deposition
ONO	Oxide-Nitride-Oxide
IC	Integrated Circuit
PV	Photovoltaic
LPCVD	Low Pressure Chemical Vapor Deposition
LP	Low Pressure
PVD	Physical Vapor Deposition
PLD	Pulsed Laser Deposition
SEM	Scanning Electron Microscopy
EDS	Energy Dispersive X-ray Spectroscopy
EBSD	Electron Backscatter Diffraction Analysis
ASTM	American Society for Testing and Materials
XRD	X-Ray Diffraction

Contents

Contents

List of Figures

List of Figures

List of Tables

General introduction

In recent decades, silicon nitride has been increasingly used in a variety of technological applications due to its chemical and physical properties, good resistance to thermal shock, resistance and chemical inertness [1,2] that meet most industrial requirements. The Si_3N_4 material exists in two stable hexagonal polymorphs (designated α[P31c]- and β[P63/m]-Si_3N_4) with very similar structures, both being obtained under conventional conditions. The α-Si_3N_4 phase is built basing on SiN_4 tetrahedrons and can irreversibly transform into β-Si_3N_4 at high temperatures, which is twice as short [3, 4]. Accordingly, β-Si_3N_4 must be produced so as by means of growth from the α-Si_3N_4 without any additives using high-annealing temperature around 1850 °C, so that the purity of the derived β-Si_3N_4 is extremely high. Since 1950s, the production of both phases has been reserved for a specific area of applications in structural materials for high-temperature engines [3]. Recently, the research requirements have been interested in the α-Si_3N_4 nanostructures in the form of nanobelts [5-7], nanowires [8], and nanoparticles [9] for MEMS devices, microelectronics, and optoelectronic applications. Despite being cheap, these crystalline structures and their nano-structuration advance also the solar cells technology as an emerging topic of research in the field of photovoltaic due to the efficient light absorption. Within the photovoltaic industry, most of the interest in silicon nitride compounds was particularly as thin films for use as passivation layers to protect semiconductor devices, as gate dielectric layers in thin-film transistors (TFT) and as insulator layers to fabricate metal-nitride-oxide-silicon (MNOS) devices [10].

The synthesis of crystalline α- and β-Si_3N_4 in thin-film and nanostructured form can be achieved by many experimental methods either directly during the deposition process or with an added annealing step. In general, traditional chemical vapor deposition (CVD) techniques lead to limited film quality due to expensive elaboration conditions [11]. Furthermore, the low temperature (CVD) in conjunction with high-temperature annealing can produce crystalline silicon nitride film and can be considered as an innovation technique [3], but for electronic applications, silicon nitride films are not free of hydrogen, which causes films degradation [12]. Commonly, CVD techniques are based on thermal decomposition and/or reaction of gaseous compounds especially the plasma-enhanced chemical vapor deposition (PECVD) that has been widely used in the semiconductor industry because it operates at lower temperatures

under gas mixtures of $SiH_4/NH_3/N_2$ by varying the ratio of NH_3 to SiH_4. In this process, the radio frequency (RF) is used to induce the plasma of ionized gas with high free electrons content. This technique is an excellent alternative for depositing a variety of high-quality silicon nitride thin films.

This Master Thesis deals with the possibility of the synthesis of crystalline α- and β-Si_3N_4 phases in thin-film as anti-reflector layers and as a passivation surface of semiconductor devices. The study shows secondary results leading to highlight the thin-films with refractive index gradient needed for photovoltaic industry. Furthermore, the formation of α- and β-Si_3N_4nano-crystals is monitored in silicon nitride films grown from semi-industrial (PECVD) of Research Center in Semi-conductor Technology for Energetic and subsequently annealed at high-temperature. Unfortunately, room temperature photoluminescence was not done for such a composite, due to the unavailability of this analysis, making it as a possible confirmation for been as an appropriate material for optoelectronic applications. The ongoing work aims to provide insight into the formation mechanism of nano-particles and to highlight its compatibility with the elaboration process. The demonstration of the structural behavior made thorough many characterization techniques, which have been adopted using, for this issue, grazing incidence X-ray diffraction (GIXRD) 2θ scans, Raman spectroscopy, field effect scanning electron microscopy (FE-SEM), ImageJ software to predict the atomic force microscopy (AFM) micrographs, and Fourier transform infrared (FTIR). Also, the electrochemical capacitance-voltage (ECV), and QSSPC are involved to the electronic properties. Finally, and for optical properties, only the UV-Vis-IR spectrophotometer is used. The obtained results in the 300-700 nm wavelength range attest that there is an elimination of multiple prominent absorption wells. Significant values of the optical band gap were determined to indicate the existence of predominant nanostructured particles.

The document is presented through four chapters, including a general introduction, general conclusion, and a list of bibliographical references. So in the first chapter, we expose the generalities about the properties and applications of thin films of Si_3N_4 material. In the second chapter, we will present some techniques for the elaboration of thin films, especially those used for the production of Si_3N_4 films and focusing on the technique of PECVD. The third chapter is devoted to the explanation of the different characterization and analysis techniques used for the study of the

physicochemical and optical characteristics of thin films. The fourth chapter is devoted to the presentation of the results obtained during the experimental work and which are compared with some researches available in the literature. Finally, we will conclude with a general conclusion that summarizes the main results of this research project.

Chapter I:

Generalities on silicon nitride properties and applications

I.1 Generalities on Silicon Nitride

This first chapter is devoted to a general description of silicon nitride. In the first part, we will present its crystalline structure proprieties and applications. Then, we will end this chapter by describing the growth mechanisms of thin films.

I.1. Motivation and background

In the current environmental context, photovoltaic is benefiting from the research efforts to reduce the cost of electricity production by direct conversion of light energy. The principle is to concentrate a large quantity of light energy on small surfaces of multi-junction with high efficiency and to reduce the reflection of light on the device surface. The improvement can be achieved only by applying an anti-reflective coating (ARC) device for hetero-junction solar cells, which presents challenges because of the wide absorption range and the need to equalize the current produced by each sub cell. Accordingly, silicon nitride deposited in low-frequency plasma-enhanced chemical vapor deposition (PECVD) is widely used in solar cells industry. Discovered in 1857, silicon nitride remained a curiosity until its commercialization in the 1950s [13] to become one of the most important material-grade ceramics currently available. Since its development in the early 1970s, silicon nitride has successfully replaced many compounds. The fabrication of silicon nitride thin films by PECVD process is an old research topic, which remains very active as attested by the literature. On 2007[14] Jean-Francois Lelievre has deposited SiN_X:H thin films on multi-crystalline substrates using LF-PECVD technique and studied their structural and optical properties. On 2013 [15], Priyambada PradhanJ reported that the deposition of Si_3N_4 film on a p-type substrate can be made by LPCVD and three Si_3N_4 samples were taken as reference. One was not annealed while the rest two were annealed at different temperatures to study their structural and electrical properties, as a result, XRD and SEM confirmed its amorphous nature. The stretch out of the C-V curve is more intense for the unannealed sample. The stretch out of the curve decreases with annealing, which depicts the decrease in interface trapped density. Recent research done by [16] I. Guler to study the optical and structural characterization of silicon nitride thin films deposited by PECVD with different flow rates. As results, Si nanoparticles was observed by means of HRTEM measurements, FTIR spectroscopy was used to confirm the decrease in Si atoms dangling bonds can be explained by formation of Si clusters in the SiN_x film

during the growth process. Ellipsometry measurements was also used to distinguish between amorphous and stoichiometric SiNx seeing the refractive index, using empirical equation proposed by Bustarret and fitting it to experimental data and the results have given 3.27 and 1.91 values, respectively, that are very similar to many results in literature.

I.2. Definitions

Silicon nitride (Si_3N_4) is a chemically inert compound, which is composed of silicon and nitrogen. It has a high strength in the wide temperature range, high fracture toughness, and is thermally stable nitride metals. It also has an outstanding wear resistance (both impingement and frictional mode), good thermal shock resistance and considerable chemical resistance properties. Its color varied from dark-grey to black and can be polished to a very smooth reflective surface indicating thicknesses linked to refractive index.

In general, silicon nitride can be prepared by many methods, for example; heating silicon powders in the presence of nitrogen gas [17] following the reaction as $\{Si(s) + 2\ N_2\ (g) \rightarrow Si_3N_4(s)\}$. But, it cannot be produced in bulk state and heated to more than 1850 °C, which is well below its melting point to avoid dissociation of silicon and nitrogen [18]. In addition to the conventional technique in which silicon nitride can also be produced, it exist different methods whose can be defined as divide route, carbo-thermal reduction of silicon dioxide in nitrogen atmosphere, low-pressure chemical pressure deposition, and plasma-enhanced chemical vapor deposition [19].

The silicon nitride (Si_3N_4) crystallizes in two stable crystallographic structures, designated α, and β phases [20] as shown in the figure I-1 and figure I-2, respectively. These phases are the most common forms of Si_3N_4 and can be produced under normal conditions of pressure and temperature. These have trigonal (Pearson symbol hP28, space group P31c, No. 159) and hexagonal (hP14, P63, No. 173) structures, respectively. In addition to these structures, the γ phase also can only be synthesized under high pressures and temperatures and has a hardness of 35 Gpa [21], which not considered in this work.
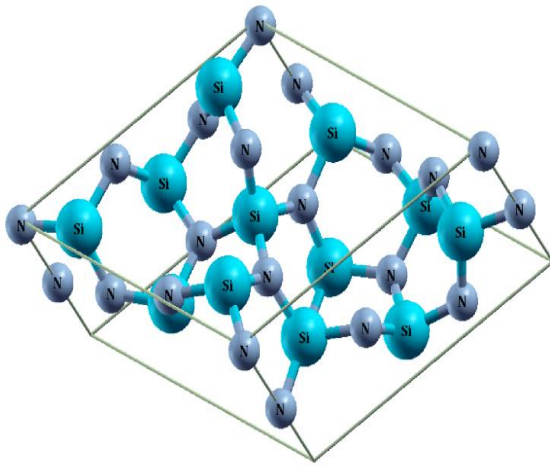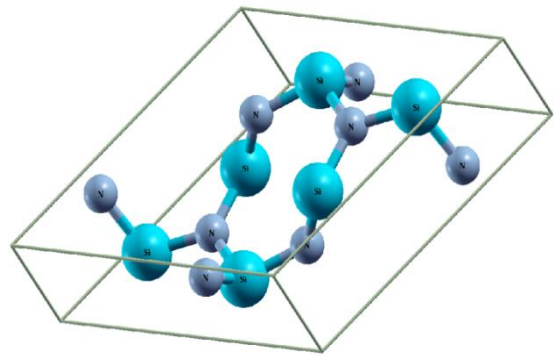
Figure I-1: Trigonal α-Si$_3$N$_4$.   **Figure I-2:** Hexagonal β-Si$_3$N$_4$.

The longer stacking sequence results in the α-phase having higher hardness than the β-phase characterized along the c axis by the periodicity of ABCDABCD otherwise to the β-Si$_3$N$_4$, which is described by ABAB stacking. However, the α-phase is chemically unstable compared with the β-phase. At high temperatures when a liquid phase is present, the α-phase always transforms into the β-phase [22]. Madelung energy calculations have indicated that β is more stable than α above 293°K, and therefore it has been suggested that transformation from α to β is possible, but not the reverse [23]. Both phases contain similar local bonding: each Si atom is tetrahedrally bonded to four N atoms (Si-N$_4$) and each N atom has a threefold trigonal coordinates (N-Si$_3$), exhibiting excellent thermal and mechanical properties combined with good wear resistance.

I.2.1. Silicon nitride properties

Table I-1 below shows the different physical properties of silicon nitride.

Table I-1: Material properties of silicon nitride.

Properties	Silicon nitride Si_3N_4
Density (kg/m^{-3})	3440
Resistivity (Ω m) at 25 °C at 500°C	~ 10^{14} ~ 2 x 10^{13}
Thermal conductivity (W cm^{-1} °C^{-1})	29
Thermal expansion (°C^{-1})	8.0 x 10^{-6}
Young′s modulus (GPa)	300
Fracture toughness (MPa m$^{-1/2}$)	0.6
Energy Gap	~5.0
Etch rate in Buffered HF(Å/min)	5-10
Refractive index	2.05
Dielectric constant	7.05
Dielectric strength (V/cm)	10^7
Infrared absorption band (μm)	11.5-12.0

I.2.2. Silicon nitride applications

The applications of silicon nitrides are given as:

1. Silicon nitride is used as passivation layer for microchips and as insulator and chemical barrier in manufacturing integrated circuits, also features asset of optical properties that makes it an ideal choice for many applications that require integration of photonic devices on chip, include ultra-high-Qresonators [24] and filters based on ultra-low-loss waveguides [25]. Silicon nitride can also be co-integrated with active components such as amplifiers [26], modulators and detectors [27]. The broad transparency window extends towards the blue wavelength range, which allows for processing visible light on chip [28,29] and biophotonic sensing applications [30].

2. Silicon nitride has many Medical applications for example in orthopedic.

3. Sintered silicon nitride is used as a material for engine parts in automobile industry.

4. Due to its hardness, thermal stability, and resistance to wear bulk, monolithic silicon nitride is used as a material for cutting tools.

5. The material is currently used in market applications for example in ball bearings used in performance bearings.

I.3. Thin Film

I.3.1. Definition

As thin-film applications, the silicon nitride layer can be ranging from a nanometer to several micrometers of thickness in which their characteristics are strongly depending on the elaboration conditions. However, its use as coating layer can adjust the properties of the substrate on which it is depositing, since thin films are nano-sized in a spatial direction, the physical and chemical properties of thin films may differ from those of low dimensional to a bulk state. So, the extreme variations of fundamental properties of materials have a link to the order of magnitude of the study allowing for example to an insulating material in a bulk state to become an electrical conductor in a thin film. To this end, many industrial productions in photovoltaic solar cells and electronic components adopt thin films technology because of its great properties.

I.3.2. Thin film formation mechanism

In a combination of nucleation and growth processes, a thin-layer can be made on a given substrate by basically following the atom-by-atom mode in which the adsorbed atoms, i.e., the ad-atoms, diffuse on the substrate surface. As this happens, the atomic islands have been nucleated and formed so that they increase in size, impinge on each other, and coalesce before forming a continuous film. At these initial growth stages, nucleation, growth, and coalescence, all set characteristic length scales of the films, such as the distribution of island sizes and separation, in turn, determine properties like electrical conductivity.

Depending on the deposition parameters and the substrate surface, there are three growth modes:

- Frank-van der Merwe growth (layer-by-layer).

- Stranski–Krastanov growth (joint islands or layer-plus-island).
- Volmer-Weber (isolated islands).

The three growth modes previously described are schematically illustrated in figure I-3.

"layer-by-layer"   "island"   "layer plus island"
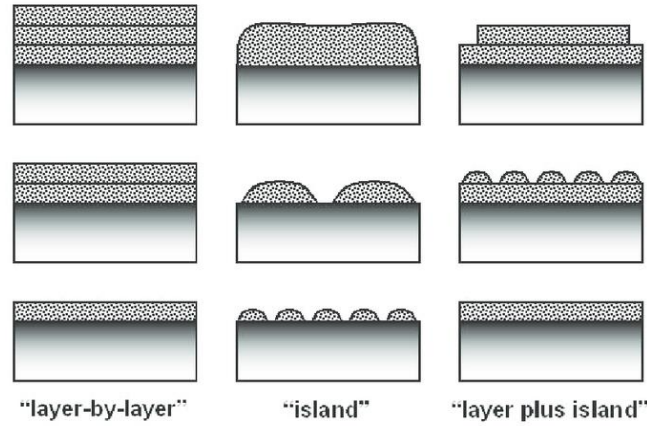
Figure I-3: Schematic illustration of the three main growth modes: " layer-by-layer " -Frank-Van der Merwe; " island " -Volmer-Weber; " layer plus island " -Stranski-Krastanov [31].

I.3.3. Deposition of silicon nitride thin film mechanism

Several reactions contribute to the formation of the silicon nitride film. In the plasma phase, many excitations, ionization, and dissociation processes take place mainly due to electron-molecule collisions, when a particle collides with a surface, it is either reflected or adsorbed. Through reactions between species present in the plasma and make clusters, they are depositing on the substrate forming that a film. Figure I-4 gives the different reaction processes of the PECVD deposition of SiN_x:H.
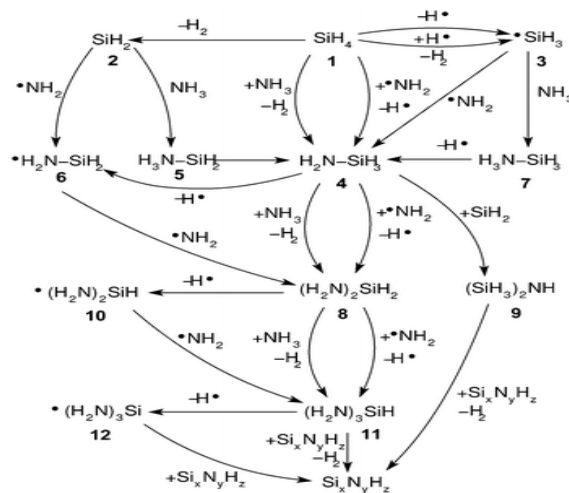
Figure I-4: Possible reactions in plasma created from a gas mixture of ammonia and silane, $Si_xN_yH_z$ represents a surface of the silicon nitride [32].

According to Dollet et al [33], there are 20 reactions compounds that will intercede in the deposition of the SiNx: H layer, some of which include:

$$SiH_3 + NH_2 \rightarrow HSiNH_2 + H_2 \tag{1}$$

$$HSi(NH_2)_2 + H \rightarrow Si(NH_2)_2 + H_2 \tag{2}$$

$$HSiNH_2 + NH_2 \rightarrow HSi(NH_2)_2 \tag{3}$$

$$Si(NH_2)_2 + NH_2 \rightarrow Si(NH_2)_3 \tag{4}$$

I.3.4. Nanostructuration of silicon nitride thin layers

Crystalline structures and their nanostructuration are an emerging research topic in the field of photovoltaic and electronic components industries, requiring the development of a wide variety of techniques to produce Si_3N_4-based nanostructures. These techniques can be divided into two categories basing on PVD (physical vapor deposition) and CVD (Chemical Vapor Deposition) [34]. Thus, the variation of these techniques leads to the synthesis of a variety of Si_3N_4 nanostructures that can be obtained for recommended applications. We note, for example, nanowires, nano-belts, nanowires, and nanoparticles. For this end, the figure I-4 shows the various Si_3N_4 nanostructures obtained by different elaboration techniques.
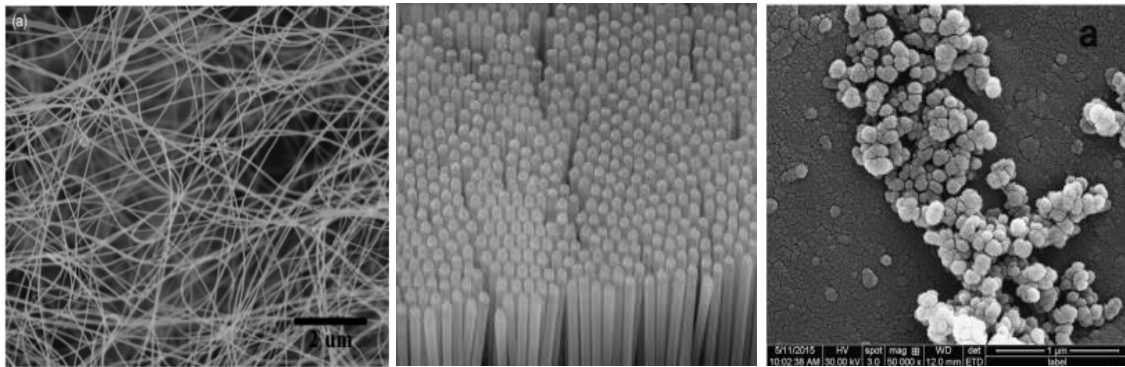
FigureI-5: Different Si_3N_4 nanostructures obtained by different deposition methods, nanofils [35] and nanobelts, nanowires [36], and nanoparticles [37].

Chapter II:

SiliconnitrideSi$_3$N$_4$

Elaboration Techniques

II. Si$_3$N$_4$ Elaboration Techniques

The formation of films on surfaces encompasses an entire field of science and engineering. The discussion below will focus on the deposition methods used for MEMS thin film deposition in electronic and photonic circuit fabrication and the description of the experimental conditions according to which this work took place.

II.1. Deposit techniques

Thin films can be made using several techniques, which are generally either a CVD (Chemical Vapor Deposition) method for depositing a solid film from chemically reactive precursor gases or a PVD (Physical vapor deposition) technique by condensing atoms in a vapor phase. Thus, CVD offers many advantages, the most important of which are low cost, excellent step coverage, uniformity, and has become the dominant technique in the industry.

II.1.1. Chemical Vapor Deposition (CVD)

Chemical vapor deposition (CVD) is a technique widely used in thin-film deposition materials like amorphous silicon, polycrystalline silicon, silicon nitride, silicon dioxide, and high-k dielectrics materials. The common factor for deposition of these different materials by CVD is that the coating is conformal [38], can coat a large number of wafers at the same time and good step coverage. So, this method is based on thermal decomposition of gaseous compounds and the desired material is directly condensing onto the surface of a substrate, therefore, the film morphology has good uniformity and coverage over a large area. Changing the source doesn't need to break the vacuum and more selective area deposition because of higher activation energy for reaction with foreign substances. For depositing these thin films, three of the most common deposition methods exist and which are [39]:

a)   Plasma Enhanced CVD

b)   Low Pressure CVD

c)   Atmospheric Pressure CVD

The choice between these different methods is making by considering several parameters such as the deposition rate, film uniformity, electrical and mechanical properties, the substrate temperature, and the chemical composition of the films. Generally, the films growth by CVD techniques follows several physicochemical stages as illustrated in Figure II-1 and which can be summarized successively as follows [40]:

1. Transport of gases from the reactor inlet to the vicinity of the deposition zone.
2. Gas phase gas reactions giving rise to the formation of precursors and by-products.
3. Transport of precursors to the surface.
4. Adsorption of precursors on the surface of the substrate.
5. Diffusion of species at the surface towards preferential growth sites.
6. Incorporation of the constituents of the film into the growing layer.
7. Desorption of the volatile products formed during the reaction and diffusion of secondary products outside the deposition zone.
8. Transport of these products to the reactor outlet.
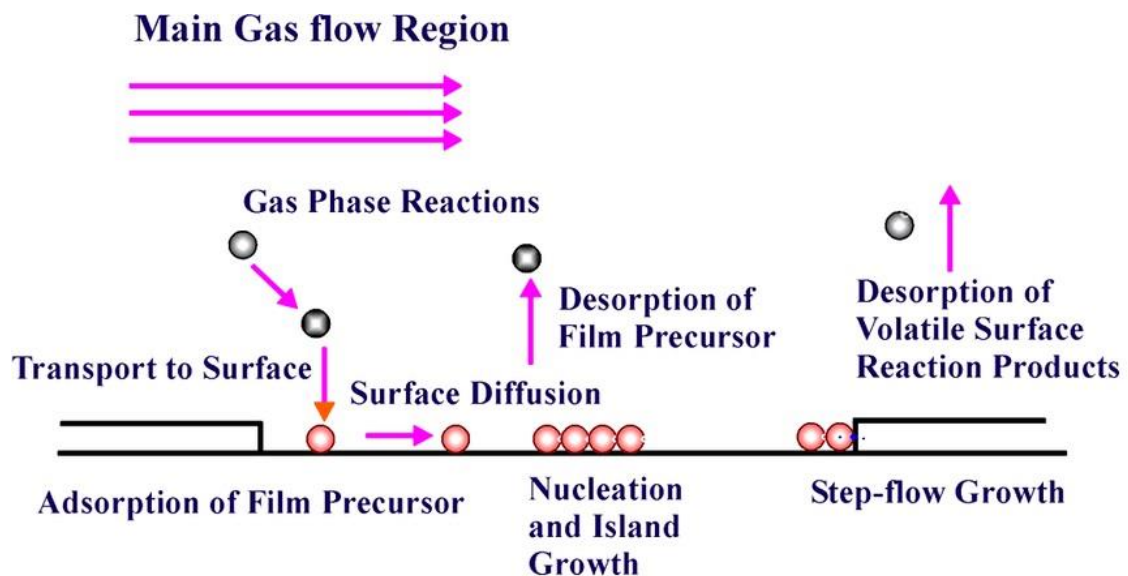
Figure II-1: Descriptive scheme of a chemical vapor deposition [41].

II.1.1.1.Plasma Enhanced Chemical Vapor Deposition (PECVD)

Plasma enhanced chemical vapor deposition is a widely accepted technique and mainly used for the deposition and the production of dielectric and passivation thin-films such as silicon oxide, silicon nitride and silicon carbide (SiC). The first reason for its acceptance resides in its operation at lower temperatures than thermally driven CVD. It was invented in 1965 by Sterling and Swann [42] and was applied to the photovoltaic industry in the mid-1970s for the production of amorphous silicon cells. Then, it was transferred in 1981, by Hezel and Schörner [43], to microelectronics and the crystalline silicon cell industry. In a technique with plasma which consists of ionized gas species (ions), electrons and some neutral species in both ground and excited states require energy for the chemical reaction so that the method can be appropriate if the diffusion of the dopant is to be kept low, the thermal budget of the treated platelets remains low with the PECVD.

The radio-frequency (RF) generator produces plasma in the reaction chamber containing reactive ions and electrons. It facilitates the film growth due to the activation energy obtaining a good grip and high growth rates. The properties of coated layers can be better influenced by PECVD than by a simple thermal deposition technique. In the PECVD, more parameters can be varied and controlled, allowing us to adjust the adhesion, stress, hydrogen content and density, etching capacity, etching rate and selectivity in etching, stoichiometry and cleanliness of the deposited layers, their thickness, and their uniformity. Indeed, two kinds of PECVD reactors, basically, can be used:

A. As shown in figure II-2, the horizontal direct PECVD is widely used in the industry, which applies an electromagnetic field to excite gases processing to produce samples. The electromagnetic field has a frequency of either 13.56 MHz (high-frequency method) or in the 10-500 kHz range (low-frequency method). Laboratory-type machines consist of two electrodes with areas typically not larger than 300 cm^2 in which the plasma excitation frequency has a strong impact on the electronic properties and the reason is that below the so-called plasma frequency (~4MHz) [44]. Indeed, ions can then follow the plasma excitation frequency and, therefore, produce a strong surface bombardment. Due to the resulting surface damage, SiN films prepared

by direct PECVD at high frequency (13.56MHz) provide much better surface passivation and a much better UV stability than SiN films prepared at low frequency [45].
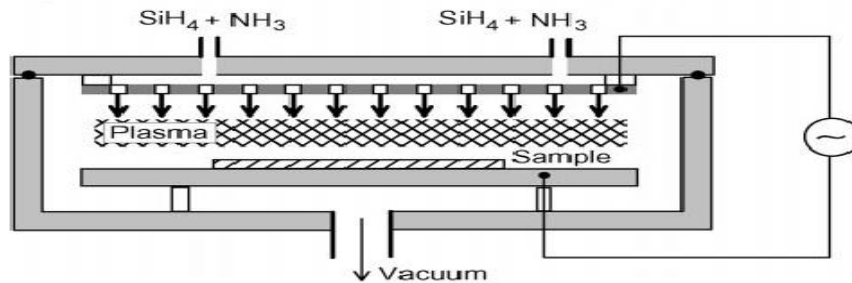
Figure II-2: Direct type PECVD reactor [45].

B. Until very recently, all commercially available high-throughput PECVD systems for the deposition of SiN into Si wafers are the so-called batch reactors. Instead of two electrodes, these reactors use a large number of electrodes connected in parallel, as shown in figure II-3.
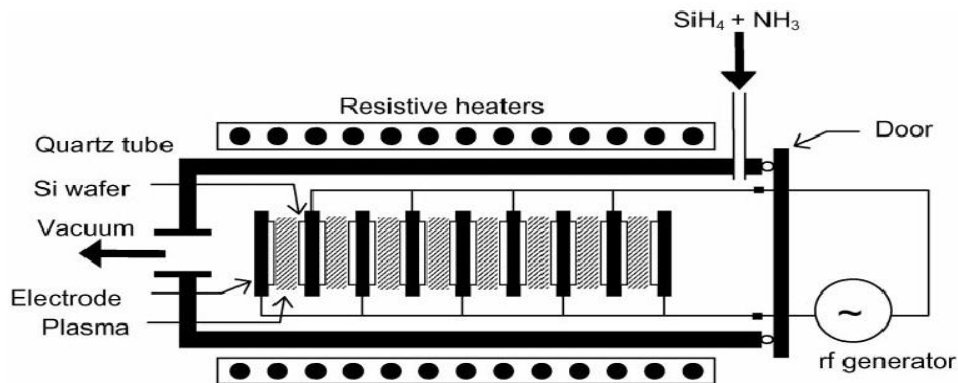
Figure II-3: Direct-plasma batch PECVD reactor [45].

C. In the remote type reactor, as shown in figure II-4, the excitation of the plasma is spatially separated from the sample. Many different plasma excitation approaches exist (microwaves, hollow cathode, arc jet, etc.). Using microwaves, the plasma excitation occurs outside the vacuum chamber, and the excited species are directed onto the sample using a

narrow quartz tube. The key advantage of the remote-plasma approach is that much higher plasma densities, and hence much higher deposition rates can be achieved compared to direct PECVD. This is an important aspect concerning the low-cost mass production.
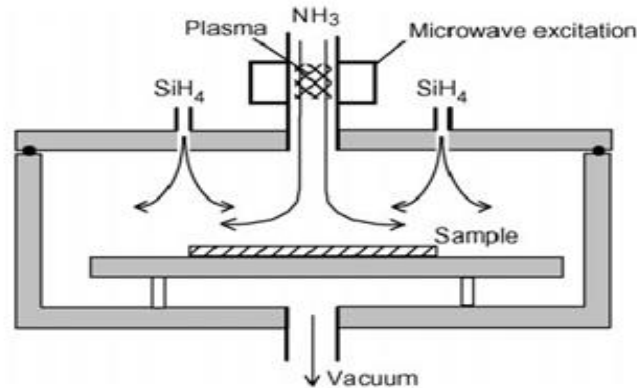
Figure II-4: Remote type PECVD reactor [45].

II.1.1.2. Low Pressure Chemical Vapor Deposition (LPCVD)

Low-pressure chemical vapor deposition (LPCVD) is a technique that uses heating temperature to initiate a reaction of precursor gases. The reaction at the substrate surface is what forms the solid phase material. Low pressure (LP) is used to decrease any unwanted gas-phase reactions, and also increases the uniformity across the substrate. Silicon-rich silicon nitride produced from Low-stress nitride shows many applications in which it can lead to making membranes that are also resistant to HF etching. Stoichiometric silicon nitride is used as an insulator, dielectric, and chemical and/or water barrier in MEMS devices, neural probes, etc.

The LPCVD process can be done in a cold or hot walled [46] quartz tube reactor. Hot walled furnaces allow batch processing and therefore high throughput. They also provide good thermal uniformity and thus result in uniform films. A disadvantage of hot wall systems is that deposition also occurs on the furnace walls, which requires more maintenance for cleaning or eventual replacement of the tube to avoid flaking of the deposited material and subsequent particle contamination. Cold wall reactors are lower maintenance, as there is no film deposition on the reactor walls.

For the LPCVD technique, as shown in Figure II-5, the tube is under low pressures ranging from 10 mTorr to 1 Torr and heated to the deposition temperature

corresponding to that of the decomposition of precursor gas. Temperatures range from 425-900°C depending on the process and the reactive gases being used. Gas is injected into the tube, where it diffuses and reacts with the surface of the substrate creating the solid phase material. Any excess gas is then pumped out of the tube and goes through an abatement system. LPCVD films are typically more uniform, lower in defects, and exhibit better step coverage that films produced by PECVD and PVD techniques. The disadvantage of LPCVD is that it requires higher temperatures, which puts limitations on the types of substrate and other materials which can be present on the samples.
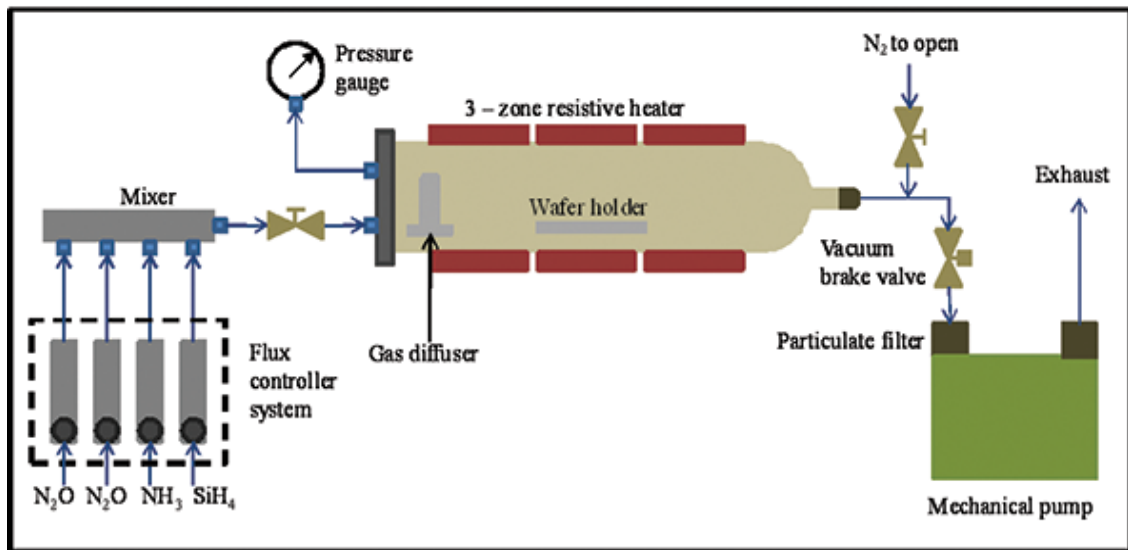
Figure II-5: Horizontal LPCVD reactor [47].

II.1.1.3. Atmospheric Pressure Chemical Vapor Deposition (APCVD)

Atmospheric pressure chemical vapor deposition (APCVD) shown in Figure II-6 is a process that occurs at atmospheric pressure (i. e. 1 atmosphere = 101,325 Pa = 760 Torr) used to deposit thin layers of specific materials (i. e. silicon nitride). APCVD is compatible with continuous in-line processes without vacuum, making it very attractive for high-volume, high-cost manufacturing applications such as PV cell manufacturing.

The deposition process begins by placing the substrates (glass wafers) on the carbon plate under vacuum chamber and then injecting the N$_2$ gas to atmospheric pressure. The deposition temperature is maintained too (830°C) [49] in the presence of

a gas precursor. By moving the carbon plate inside the muffle, the glass substrate traverses underneath the coater and thin-films are deposited.
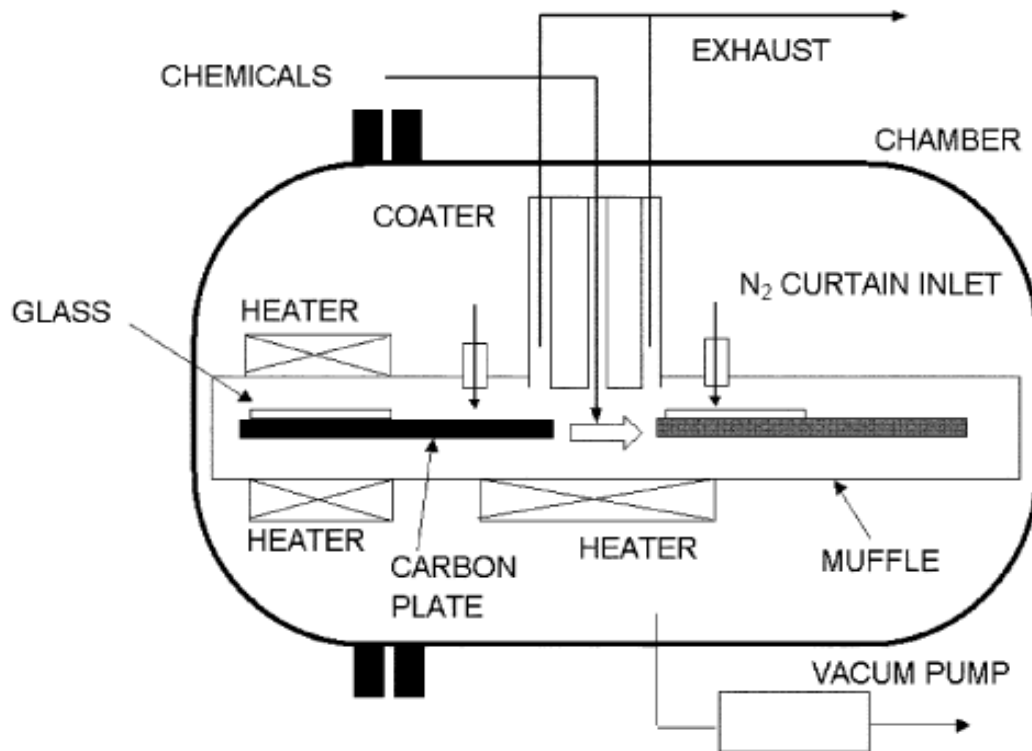
Figure II-6: Scheme of an APCVD reactor to deposit thin layer of silicon nitride on glass [49].

II.1.2. Pulsed Laser Deposition (PLD)

Pulsed laser deposition (PLD) technique stands as a simple, versatile, rapid, and cost-effective method, which can enable precise control of thickness and morphology for the fabrication of high-quality films [49,50]. Where high-power pulsed laser beam is focused inside a vacuum chamber to strike a target of the material that is to being deposited. The atoms and ions ablated from the target(s) are deposited on substrates (such as a silicon wafer facing the target) shown in figure II-7. Mostly, the substrates are attached with the surface parallel to the target surface at a target-to-substrate distance of typically 2–10 cm. This process occurs in an ultra-high vacuum or in the presence of oxygen gas, which is commonly using when depositing material oxides.

The process of PLD can generally be divided into four crucial stages assuring crystallinity, uniformity, and stoichiometry:

A. Laser absorption on the target surface and Laser ablation of the target material and creation of a plasma.
B. Dynamic of the plasma.
C. Deposition of the ablation material on the substrate.
D. Nucleation and growth of the film on the substrate surface.
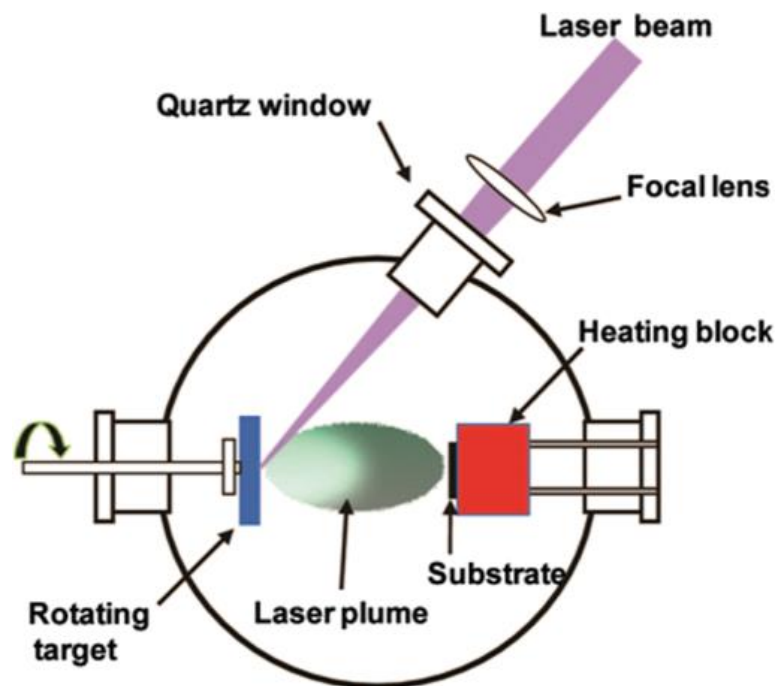
Figure II-7: Schematic illustration of the pulsed laser deposition (PLD) [51].

II.1.3. Nitration method

Nitration is a surface treatment that consists of incorporating nitrogen into the thin film to modify these physicochemical properties. This process consists of placing the silicon wafer in a very high-temperature furnace of 1300°C to 1400°C under nitrogen atmosphere. The nitrogen then diffuses to the surface of the thin-film, creating a bifocal nitride layer if the rear side of the wafer is not covered.

$$3Si + 2N_2 \rightarrow Si_3N_4.$$
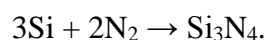
The mass of the silicon sample gradually increases as the nitrogen attaches to the material to form nitride. In the absence of an iron-based catalyst, the reaction ends after a few hours (about seven hours), which means that the mass of the silicon sample stops

growing, indicating that the nitrogen no longer binds to the silicon. In addition to Si$_3$N$_4$, various other silicon nitride phases are formed, such as gaseous Si$_2$N di-siliconmono-nitride, SiN silicon mono-nitride and Si$_2$N$_3$ silicon nitride, each of which corresponds to a stoichiometric phase. As is the case for other refractory materials, the products obtained by these high temperature processes depend on the reaction conditions (time, temperature, starting materials, possible adjuvants, container materials, etc.) as well as the mode of reaction of purification.

II.2. Elaboration of Si$_3$N$_4$ thin films

Before being introduced into the PECVD reactor shown in the figure II-8, the silicon substrates must be cleaned chemically so that surface pollutions, in particular the native oxide, do not disturb the deposition process.

II.2.1. Chemical treatment

The quality of the deposits depends on the surface condition and the cleanliness of the substrate in question. The surface must be thoroughly cleaned to remove any traces of impurities and grease. This cleaning, carried out in our clean room, comprises three phases:

- H$_2$SO$_4$ /H$_2$O$_2$ for 10-15min at 80°C.
- HCl/ H$_2$O$_2$ at ambient temperature.
- HF (10%) for 20s.

The silicon substrates are then quickly placed in the reactor.

II.2.2. Layer deposition

Si$_3$N$_4$films were deposited on monocrystalline silicon wafers, 340-370μm thickness oriented (100).In this study the p-type wafers are placed vertically in the PECVD direct-plasma batch reactor developed by SEMCO Engineering on the graphite electrodes that serve as a support for the samples, the contacts located between the substrate and the electrodes lead to better deposition homogeneity. Then, SiN$_x$ films were immediately deposited using a mixture of silane and ammonia. The vacuum reaches a residual pressure of 1750 torr then we inject Argon gas for 15 min and we

create radiofrequency plasma with the power of 4500 Watt by adding the precursor gases silane SiH$_4$ and ammonia NH$_3$, see table II-1.

The same protocol is followed for all the samples deposit series, taking into account the change of the parameters mentioned in the table II-1.

TableII-1: Elaboration conditions.

Samples	color	Time deposit	Temperature deposit (°C)	Pressure (Torr)	Power(W)	R= NH$_3$/SiH$_4$
A	green	10 mn	450	1750	4500	2.500
B	purple	4 mn	485	2000	5000	2.143
C	Light blue	150 s	500	1750	4500	2.333
D	blue	120 s	500	1750	4500	2.143

Figure II-8: PECVD reactor (CRTSE).

After the deposition, samples will undergo two steps of heat treatment at 1150°C to study their consequences on the silicon nitride properties and to understand the behavior of phase separation in Si$_3$N$_4$ thin films.

II.2.3. Heat treatment

In this study, silicon nitride films were annealed twice in a Tempress furnace at 1150°C under a nitrogen atmosphere instead of 1850°C, but because of the lack of the necessary equipment to do this annealing; we opted for another method that will give us the hopping result, the annealing equipment being available in our cleanroom.

This operation is done by raising and lowering the temperature at different temperatures and durations, shown in figure II-8.
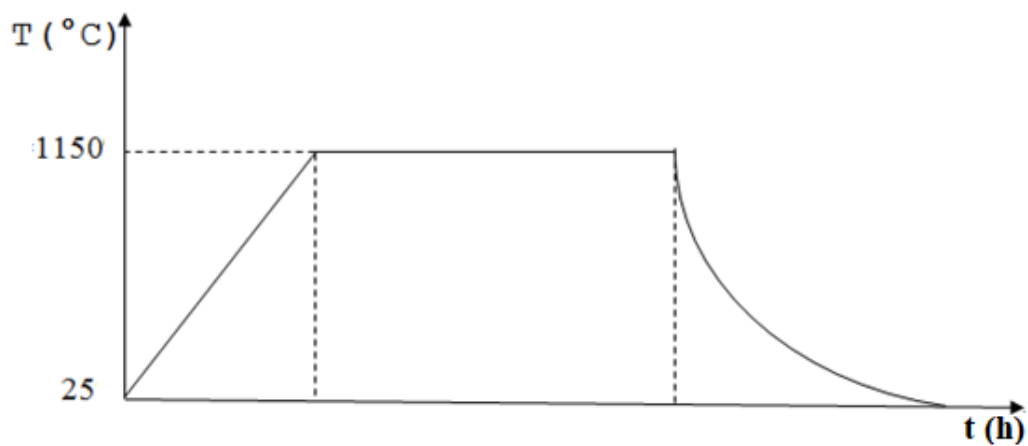
Figure II-9: Thermal cycle established for the annealing of sample.

The annealing of the thin layers makes it possible to eliminate the organic species present in the starting solution, to condense and homogenize the material, crystallizes the resulted films.

Chapter III

CharacterizationsTechniques

III. Si$_3$N$_4$ Characterization Techniques

There are many characterization techniques that can give information about the samples to known the structure, composition, morphology, topography and other various properties of the prepared sample characterization. In this chapter, we will describe the principle technique used for the characterization of the thin films used in this study.

III.1. X-ray Diffraction (XRD)

X-ray diffraction is a nondestructive fast and easy sample prepared technique that can be done in-situ that gives detailed information about the chemical composition and crystallographic structure for a single crystal, poly, and amorphous materials. X-ray diffraction is used to identify crystalline phases and orientation of a single crystal or grain to measure the size, shape and internal stress of small crystalline regions and thickness of thin films and multi-layers. By this technique we can determine the average spacing between layers or rows of atoms and the atomic arrangement.

For the X-rays to yield useful information about the structure, the wavelength of the incident X-rays should be of the same order of magnitude as the interatomic distance. The dominant effect that occurs when an incident beam of monochromatic X-rays interacts with a target material is scattering of those X-rays from atoms within the target material, shown in figure III-1.

The principle of this method is based on the Bragg law, which is defined by the relation:

Bragg's Law:

$$n \lambda = 2 \, d \, \sin (\theta)$$

where

λ is the wavelength of the rays

θ is the angle between the incident rays and the surface of the crystal

d is the spacing between layers of atoms

and constructive interference occurs when n is an integer (whole number)
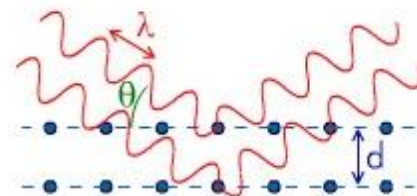
Figure III-1: X-ray Diffraction for Bragg's condition.

These X-rays are generated by a cathode ray tube, filtered to produce monochromatic radiation, collimated to concentrate, and directed toward the target material. In this type of Diffractometer D8 Advance Brucker shown in figure III-2, the detector is based on a speed rotation motion $2\omega = 2d\theta$ dt. The detector, therefore, rotates by an angle 2θ while the goniometer carrying the sample rotates by an angle θ. An angle scan is then performed. When an angle θ corresponding to a family of planes (hkl) where the Bragg relation is satisfied ($n\lambda = 2d \sin \theta$), the detector records an increase in the diffracted intensity. After the detection of the photons, the counter transforms them into electric charge, and then they are amplified by an electronic system. The electrical signal is sent to a computer which gives the appearance of the spectrum with different diffraction peaks.

Figure III-2: Diffractometer D8 Advance Brucker (CDTA).

III.2. Field effect scanning electron microscopy (FE-SEM)

A Scanning electron microscope is a technique used in surface analysis. It analyzes the morphology of the surface and the chemical composition of the solid matter by scanning the surface with a focused beam of electrons (probe) that scans point by point and line by line the surface of the object. Various interactions between incident electrons (primary) and matter generate different signals some of which (electrons) are used to construct images and others (RX) for chemical microanalysis.

The scanning electron microscope uses two types of electrons, secondary and backscattered electrons, each of which can be detected by specialized detectors. Backscattered electrons are a result of an elastic collision and scattering between incident electrons and specimen nuclei or electrons. Secondary electrons are a result of the inelastic collision and scattering of incident electrons with specimen electrons.

SEM work under high vacuum, however, for electrically insulating samples, these may need to be coated with gold or graphite to stop charge building up on the surface. The resolution of SEM can fall somewhere less than 10 nm.
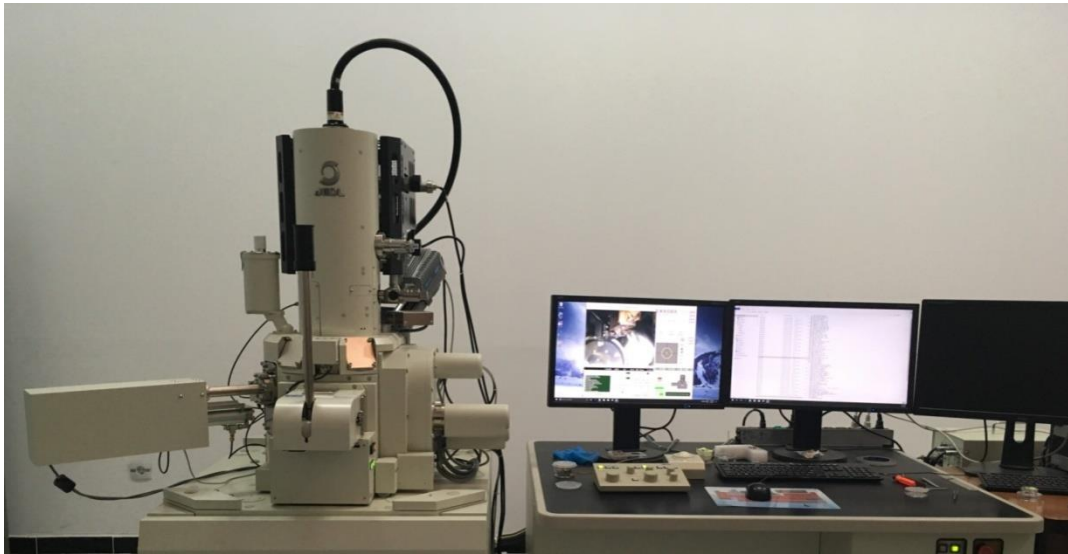
Figure III-3: Field effect scanning electron microscope (CRTSE).

In our analysis, we used an ultra-high-resolution Schottky Field Emission Scanning Electron Microscope developed by JEOL shown in figure III-3. A unique electron optical system allows a variety of analyses and observation at high magnification which has semi-in-lens objective lens shown in the figure III-4 and High Power Optics of the irradiation system deliver observation with high-spatial-resolution

and stable analysis capability. Furthermore, Gentle Beam mode can reduce the incident electron penetration to the specimen, enabling you to observe its topmost surface by using a few hundred landing energy and can achieve a better resolution (15 kV 0.8 nm, 1 kV 1.0nm) and provide all the performance you need to conduct everything from high-magnification viewing to EDS and EBSD analyses.
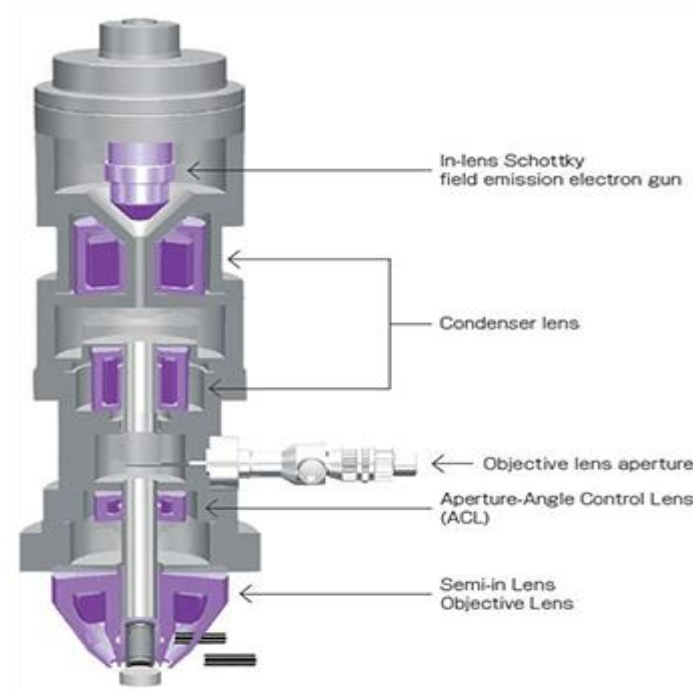
Figure III-4: Schematic diagram of field effect scanning electron microscopy.

III.3. Raman spectroscopy

Raman spectroscopy shown in figure III-6 and Raman microspectroscopy is non-destructive methods of observing and characterizing the molecular composition and external structure of a material, which exploits the physical phenomenon in which a medium slightly modifies the frequency light circulating there. This frequency shift says the Raman effect corresponds to an exchange of energy between the light ray and the medium and gives information on the substrate itself. Raman spectroscopy involves sending a monochromatic light onto the sample and analyzing the scattered light. The information obtained by the measurement and the analysis of this shift makes it possible to go back to certain properties of the medium, by spectroscopy.

The quantum theory approach shown in figure III-5 to Raman scattering recognizes that the vibrational energy of a molecule is quantized. A non-linear

molecule will have 3N-6 normal vibrations and a linear molecule will have 3N-5, where N is the number of atoms in the molecule. The energy of each of these vibrations will be quantized according to the relationship [52]:

$$Eg = hv(v + 1/2) \qquad (1)$$
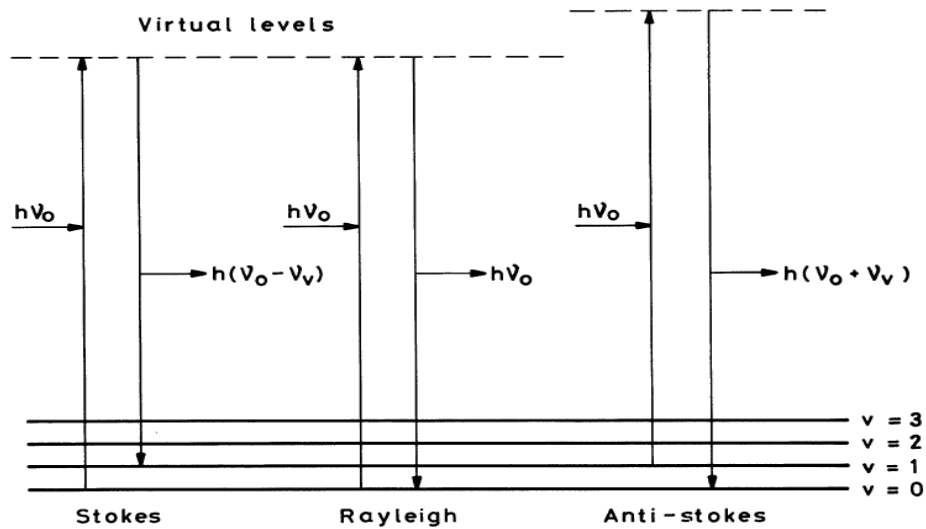
Figure III-5: Idealized model of Rayleigh scattering and Stokes and anti-Stokes Raman scattering [52].

Figure III-6: Raman spectroscopy (CDTA).

III.4. Surface roughness from SEM images using Image J software

ImageJ is cross-platform image processing and analysis software developed by the National Institutes of Health in 1987. The most common image processing operations can be performed with ImageJ many operations like viewing, adjusting the grayscale histogram, denoising, lighting correction, edge detection, direct and inverse Fourier transformation, thresholding, logical operations and arithmetic between images, and in general, any type of linear transformation by custom definition of masks. Also, it can count particles, evaluate their aspect ratios, measure various quantities (distances, surfaces), extract contour coordinates, etc.

ImageJ was originally developed for biomedical applications and used in materials science for the determination of grain sizes and processing image obtained by X micro-tomography. With the unavailability of some characterization instruments, particularly the AFM, this software can simulate surface roughness graphs by processing SEM images.

III.5. Ultraviolet–visible spectroscopy

Ultraviolet-visible spectroscopy is an optical characterization technique relies on the interaction of electromagnetic radiation and matter that results in some absorption, transmission, and reflection of light over a certain range of wavelength UV-Visible (200-800 nm). It's a non-destructive technique that requires no preparation of the samples. Spectrophotometer shown in the figure III-7 is made of a Deuterium lamp that emits a continuous spectrum in the ultraviolet region (190-400 nm) and Tungsten lamp (emitting in the 400 to 800 nm) (visible), support for the sample, a monochromator and a detector.
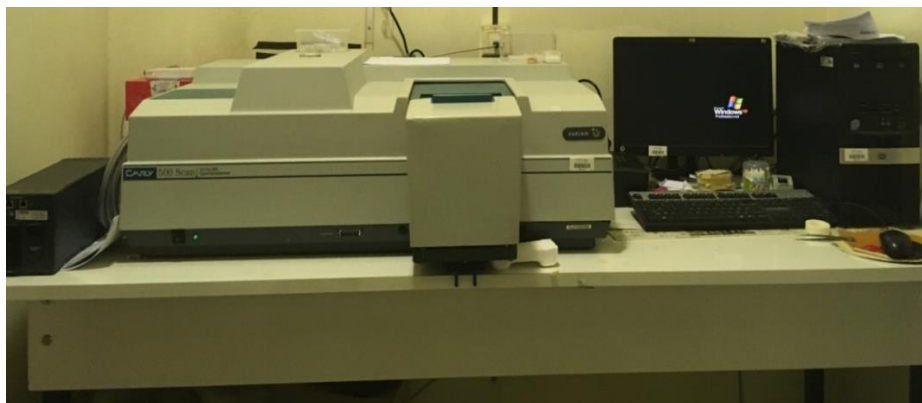
Figure III-7: Spectrophotometer (CRTSE).

A beam of light from a visible /UV light source will go through the sample over a short period; the spectrometer automatically scans all the component wavelengths and produces a graph that relates the absorbance to the wavelength in the visible and ultraviolet regions.

The operating principle of the spectrophotometer is shown in the figure III-8:
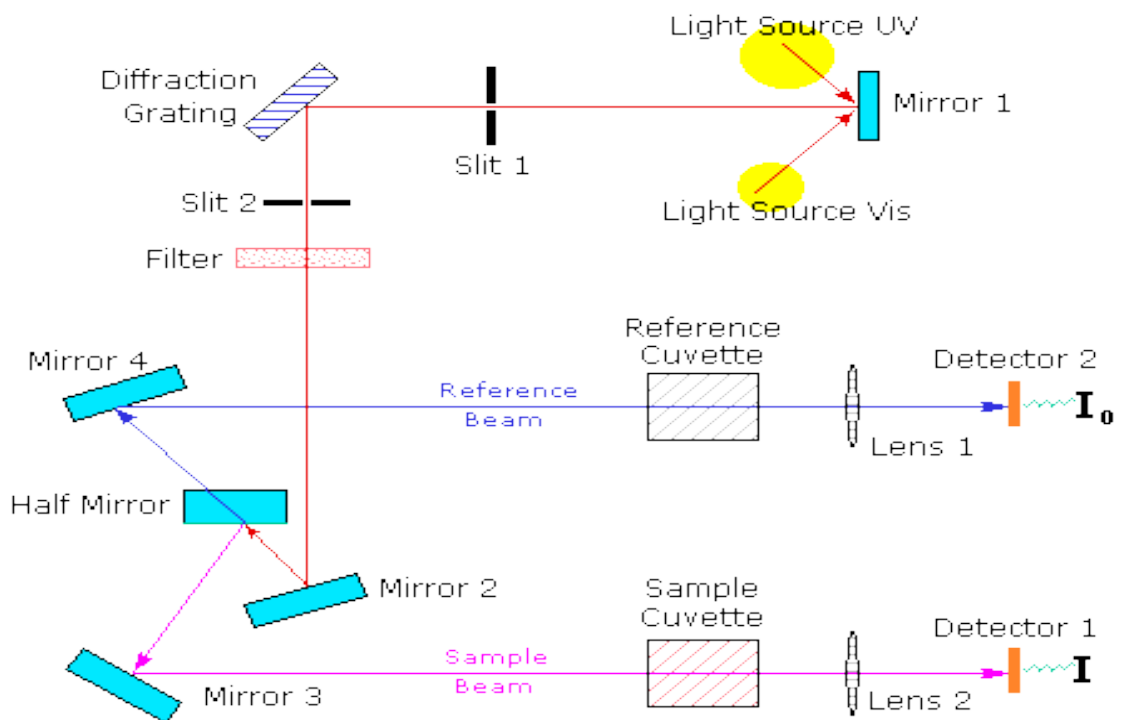
Figure III-8: Schematic diagram of the spectrophotometer.

III.6. Wafer lifetime measurement

The WCT-120 is tabletop silicon lifetime and wafer metrology system suitable for both device research and industrial process control. It's a non-destructive technique that requires no preparation of the samples and it is ideal for monitoring multi-crystalline wafers, dopant diffusions, and low-lifetime samples. This method complements the use of the transient photo-conductance technique. The quasi-steady-state photo-conductance (QSSPC) lifetime measurement also yields the implied open-

circuit voltage (versus the illumination) curve, which is comparable to an I-V curve at each stage of a solar cell process. The operating principle of the Sinton WCT-120 is shown in figure III-9:
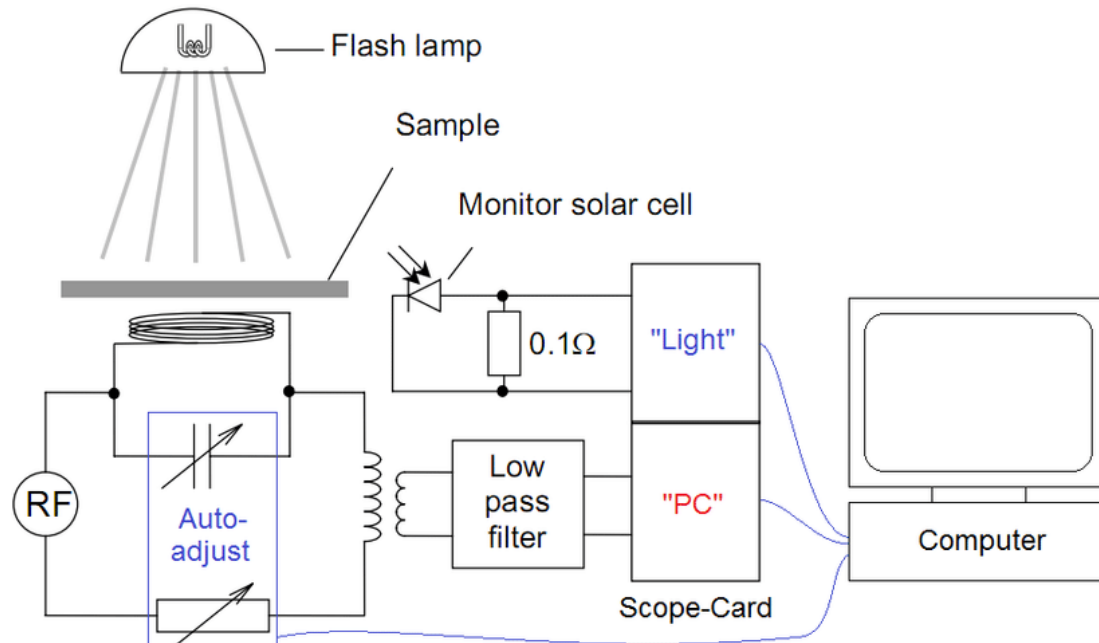
Figure III-9: Schematics of the Sinton WCT-120 series QSSPC instrument [53].

Chapter IV

Results and Discussions

IV. Results and Discussions

In this chapter, we present the structural, morphological and optical characterizations results obtained from the deposed thin-films of silicon nitride.

IV.1. XRD spectrum of Si_3N_4 thin film

The XRD characterization was done using a Bruker D8 Advance type Diffractometer, where x-ray radiations are produced from copper K_α emission source. The material and structure were determined by comparing the spectra obtained with the database called ASTM (American Society of Testing Materials) using High-Score Plus.

Figure IV-1 assemblies all the X-ray diffraction spectrum of the Si_3N_4 thin films of sample A as deposited on substrates and heated twice to 1150°C.

The XRD measurements for as-deposited film denoted A_1 shows several peaks so that sharp-prominent peaks correspond to β-Si_3N_4 and was compared with the Si_3N_4 data reported in data sheet with Reference code: (96-100-1248) and the other peaks correspond to α-Si_3N_4 compared with (ASTM data sheet Reference code: 96-100-1240) [45,55] which almost mush. In the second XRD spectrum denoted A_2, the film was heated to 1150°C and we notice a formation of new peaks that have no relation to the previous one and the appeared (011); (110); (301); (031) peaks are more intense and remain the same with a small shift of 0.9°, we conclude that the material formation has a preferential orientation. As for the third XRD spectrum A_3, the film is annealed to 1150°C for the second time and we have noticed a decrease in peaks number within attenuation of the beta phase formation except a formation of a small peak (500). The appearance for new peaks (203); (303) are assigned to the α-Si_3N_4 phase and compared with (ASTM data sheet of Reference code: 96-100-1247). In this sample, both of α and β structures have coexisted [56] with a dominant presence of the alpha phase.
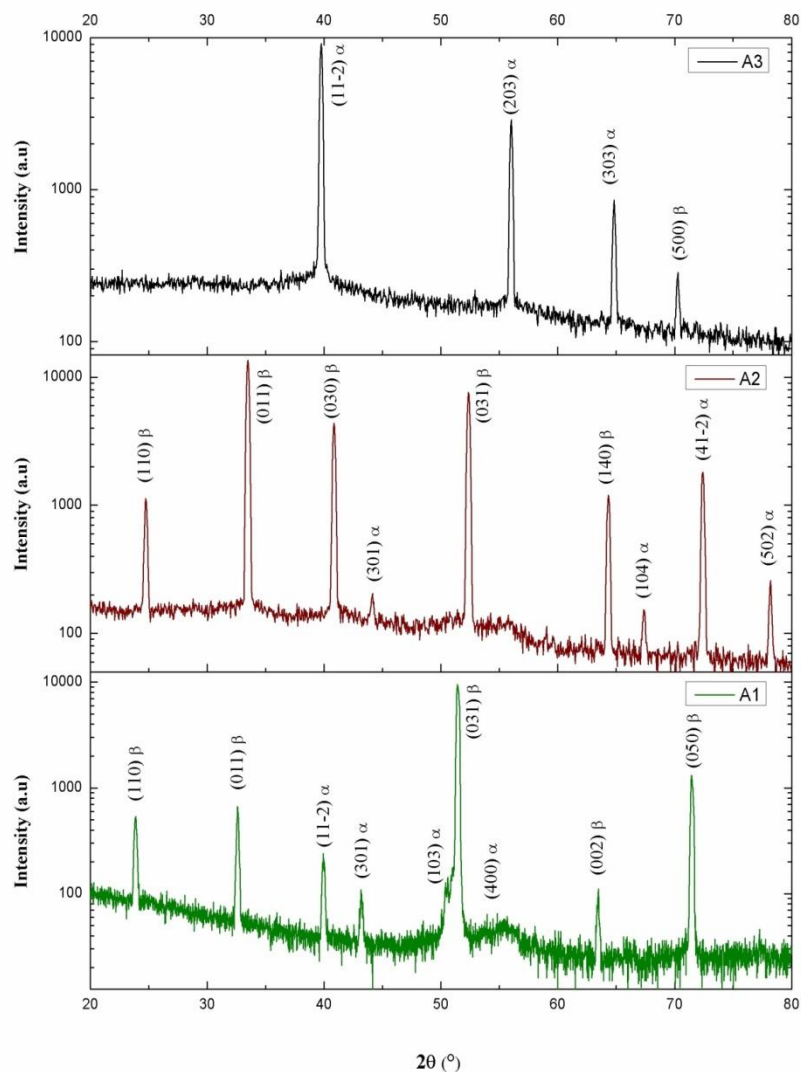
Figure IV-1: XRD pattern of Si_3N_4 films of sample A considering the case of as deposited and annealed at 1150°C, once and twice.

Figure IV-2 groups all the X-ray diffraction spectrum of the Si_3N_4 thin films of sample B as deposited on substrates and heated twice to 1150°C.

As for the B sample, the as-deposited film denoted B_1 shows sharp prominent peaks correspond to β-Si_3N_4 complementing with (ASTM data sheet reference code: 96-100-1240) and the least intense peaks correspond to α-Si_3N_4 compared with (ASTM data sheet reference code: 96-100-1246) [45,55]. After that, the second XRD spectrum denoted B_2 is assigned to the film, which is heated at 1150°C. We notice, in this situation, some previously appeared peaks are missing due to the formation of new peaks as (101); (21-1); (400); (213); (051) corresponding to α-Si_3N_4 compared with (ASTM data sheet reference code: 96-100-1242). We have also obtained (031); (330);

(051) peaks corresponding to β-Si$_3$N$_4$ compared with (ATSM data sheet reference code: 96-100-1250). As for the third XRD spectrum B$_3$, the film was annealed to 1150°C for the second time and we notice reappearance of the (301) and new peaks (002); (11-2); (311); (410); (004); (421) corresponding to α-Si$_3$N$_4$ agreed with (ASTM data sheet reference code: 96-100-1241). The (050) peak corresponds to β-Si$_3$N$_4$found in (ATSM data sheet reference code: 96-100-1247). We notice that in each step of the process, the density of existence of the beta phase decrease due to the applied conditions favoring the formation of the alpha phase.
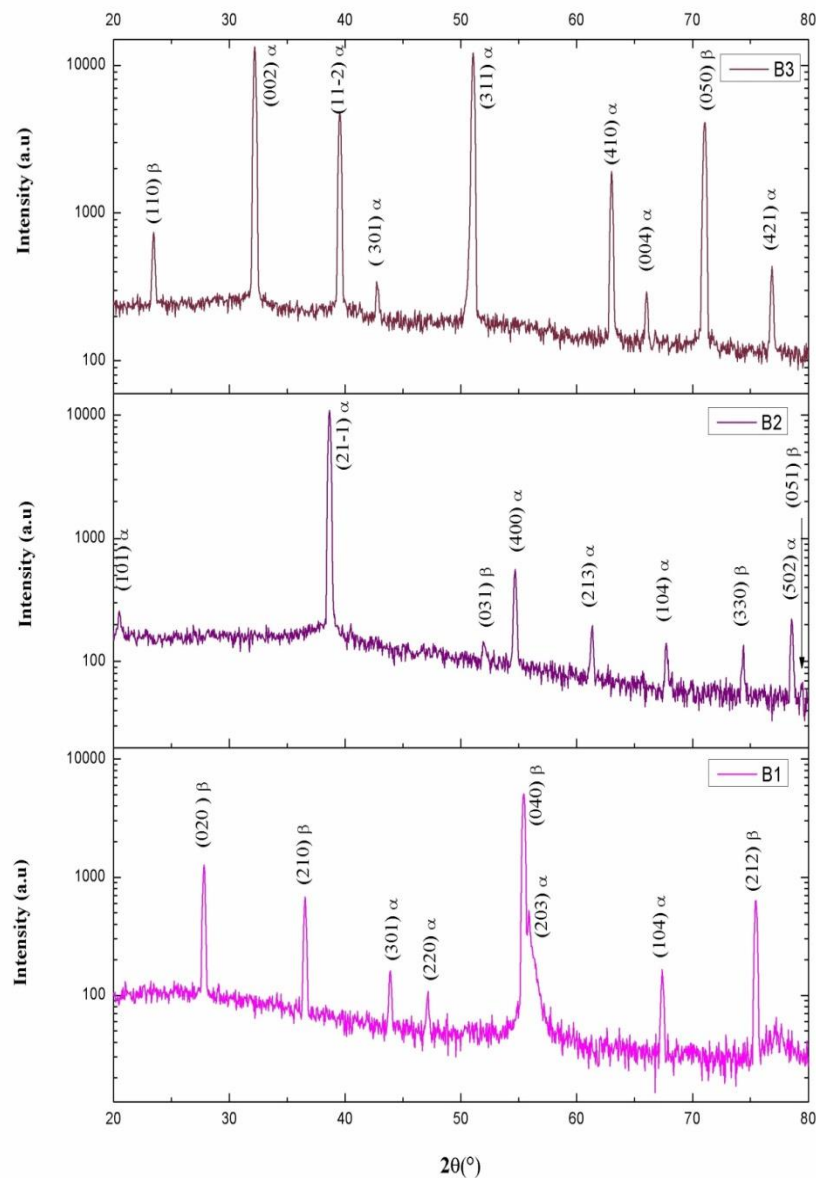
Figure IV-2: XRD pattern of Si$_3$N$_4$ films of sample B considering the case of as deposited and annealed at 1150°C, once and twice.

IV. Results and Discussions

Figure IV-3 groups all the X-ray diffraction spectrum of the Si_3N_4 thin films of sample C as deposited on substrates and heated twice to 1150°C. From the C-sample XRD measurements, the as-deposited film denoted C_1 shows several peaks corresponding to α-Si_3N_4 and was compared with the Si_3N_4 data reported in datasheet with reference code : (96-100-1244) and one peak corresponds to β-Si_3N_4 comparing with (ASTM datasheet reference code: 96-100-1247) [45,55], which almost much. In the second XRD spectrum denoted C_2, the film was heated to 1150°C. We notice a formation of new peaks that have no relation to the previous peaks (200); (002); (301); (32-2) corresponding to α-Si_3N_4 agreeing with (ASTM datasheet reference code: 96-100-1244) and (031); (311); (330) peaks correspond to β-Si_3N_4 comparing with (ATSM datasheet Reference code: 96-100-1250) the peak (21-1) remains unchanged. As for the third XRD spectrum C_3, the film was annealed to 1150°C for the second time, therefore, we notice the reappearance of (301); (220) peaks, but some other peaks are missing due to the formation of new peaks as (020) (104) corresponding to α-Si_3N_4. The appeared (210); (040); (022); (212) peaks are assigned to β-Si_3N_4regarding the (ASTM datasheet reference code: 96-100-1250). In this sample, both of α and β structures have coexisted [56].
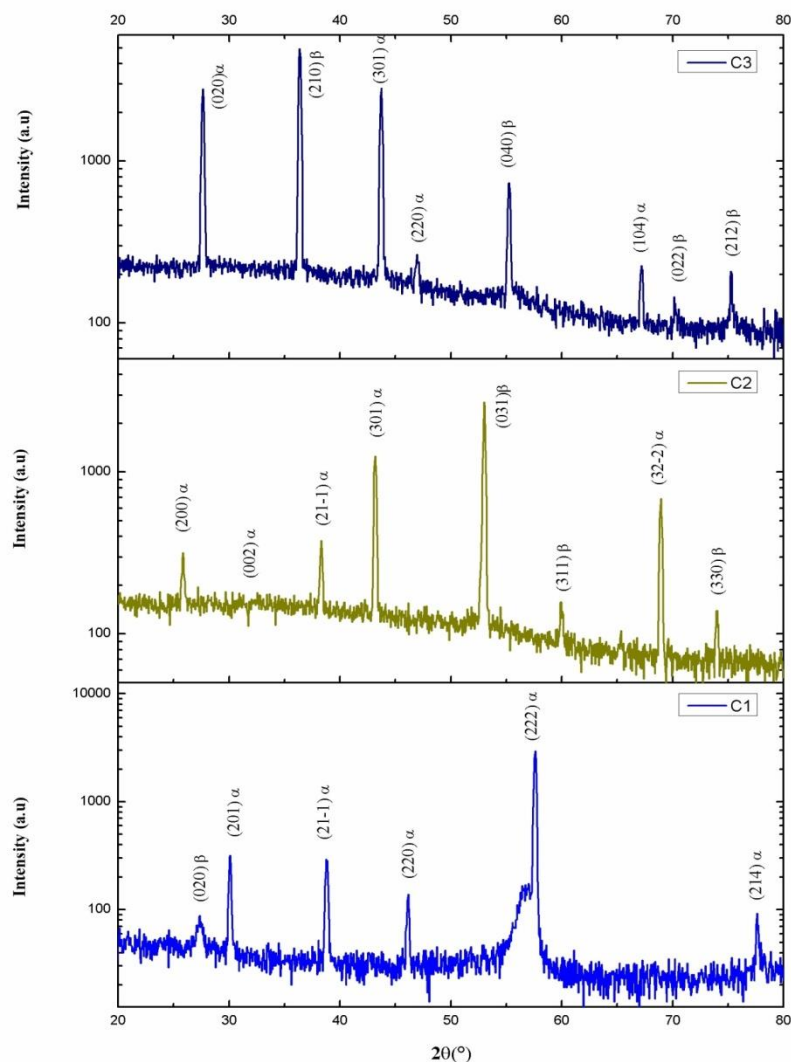
Figure IV-3: XRD pattern of Si_3N_4 films of sample C considering the case of as deposited and annealed at 1150°C, once and twice.

Figure IV-4 groups all the X-ray diffraction spectrum of the Si_3N_4 thin films of sample D as deposited on substrates and heated twice to 1150°C.

Finally, for D sample, the as-deposited film denoted D_1 shows several peaks so that the sharp-prominent peaks correspond to α-Si_3N_4 and was compared with data reported in data sheet with reference code: (96-100-1241) and to a β-Si_3N_4data sheet reference code: (96-100-1245) [45,55], which almost increased in density. As for the second XRD spectrum D_2 assigned to the heated film, we noticed that the number of peaks has increased with a formation of new peaks (200); (21-1); (11-2); (311); (320); (004), (330); (214) corresponding to α-Si_3N_4 complementing with (ASTM datasheet

reference code: 96-100-1240) and (130), peaks correspond to β-Si₃N₄. As for the third DRX spectrum D₃, the film was annealed to 1150°C for the second time and we notice the reappearance of (200), and a formation of new peaks (102); (202); (411); (400) corresponding to α-Si₃N₄ and (411); (051) peaks are assigned to β-Si₃N₄. We have always noticed the presence of an impurity linking to N₂ (022) compared with (ASTM datasheet reference code: 96-152-7604). So, the applied conditions favored the formation of the alpha phase.
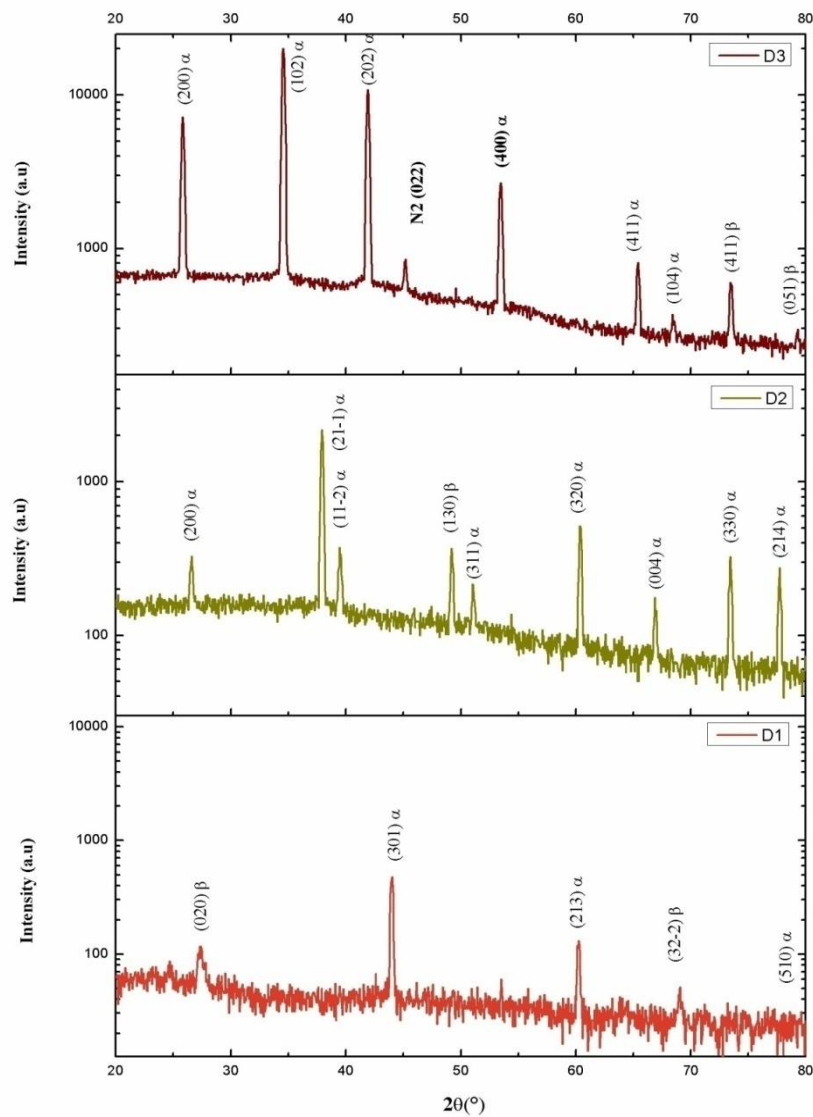
Figure IV-4: XRD pattern of Si₃N₄ films of sample D considering the case of as deposited and annealed at 1150°C, once and twice.

IV.2. Raman results

Raman spectroscopy as explained in chapter III allows us to identify molecules vibration and to study the chemical bonding and intermolecular bonds, therefore, all samples were analyzed in all stages, from deposition to annealing step learning the mechanics of formation and try to understand the material behavior.

The data were treated using Origin-Pro 8 software so that each sample was presented with stacked curves to facilitate the view of any transformation. The curves were compared to the theoretical data [57] collected in the table below:

Table IV-1: Theoretical resonance of Raman in Si_3N_4.

Alpha Si_3N_4	Beta Si_3N_4	Alpha Si_3N_4	Beta Si_3N_4
153 nm^{-1}	X	537 nm^{-1}	X
X	144 nm^{-1}	569 nm^{-1}	X
X	186 nm^{-1}	601 v	X
202 nm^{-1}	X	X	619 nm^{-1}
X	210 nm^{-1}	667 nm^{-1}	X
X	229 nm^{-1}	691 nm^{-1}	X
231 nm^{-1}	X	X	732 nm^{-1}
258 nm^{-1}	X	763 nm^{-1}	X
282 nm^{-1}	X	848 nm^{-1}	X
298 nm^{-1}	X	X	865 nm^{-1}
306 nm^{-1}	X	868 nm^{-1}	X
321 nm^{-1}	X	914 nm^{-1}	X
337 nm^{-1}	X	X	928 nm^{-1}
356 nm^{-1}	X	X	939 nm^{-1}
361 nm^{-1}	X	951 nm^{-1}	X
383 nm^{-1}	X	975 nm^{-1}	X
391 nm^{-1}	X	1032 nm^{-1}	X
X	451	X	1047 nm^{-1}
460 nm^{-1}	X	1107 nm^{-1}	X
480 nm^{-1}	X	1142 nm^{-1}	X
514 nm^{-1}	X	X	X

Figure IV-5: groups all the Raman spectra of the Si_3N_4 thin films samples as deposited on substrates and heated twice at 1150°C.

IV. Results and Discussions
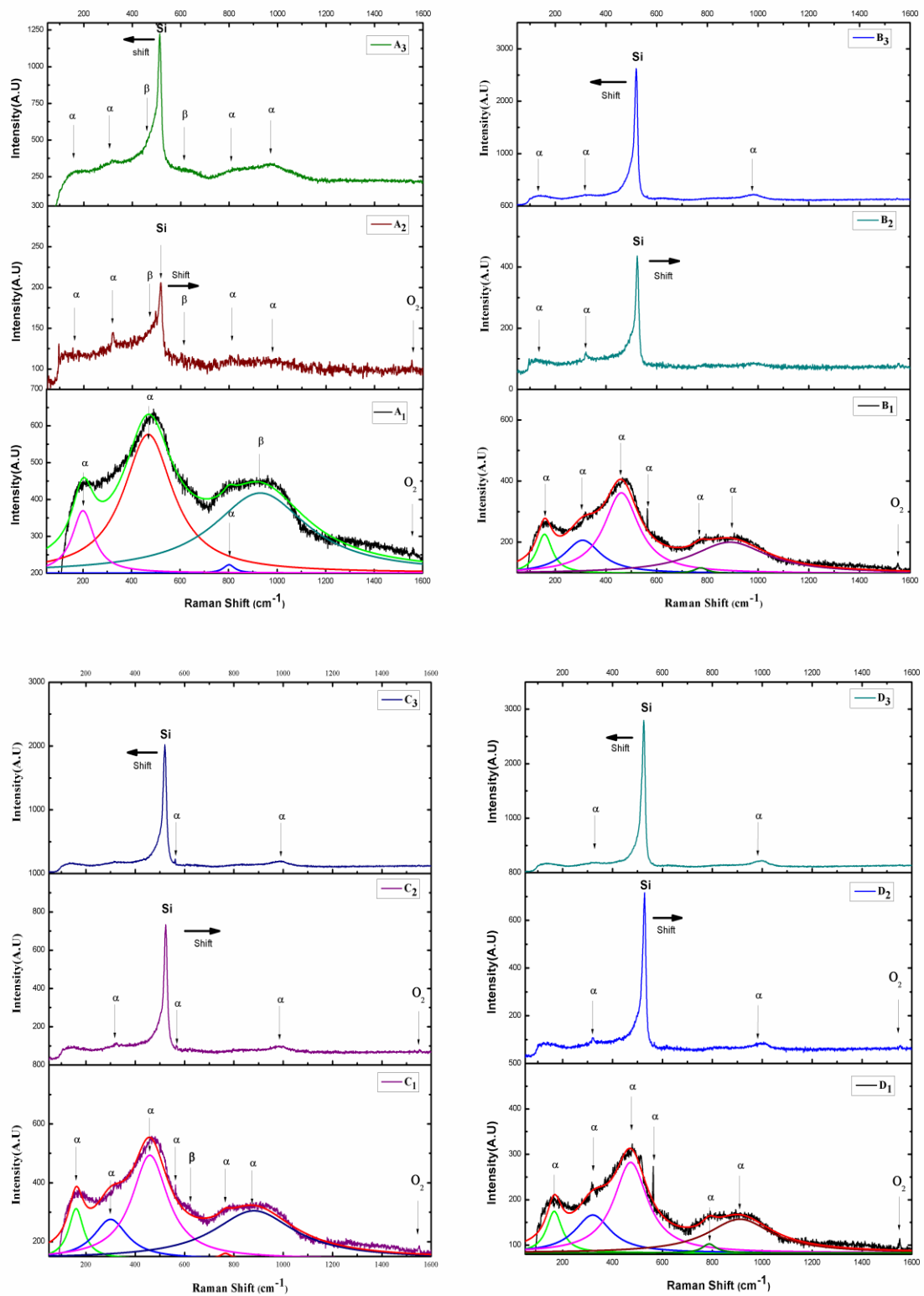
Figure IV-5: Raman spectrum of all samples considering the case of as deposited and annealed at 1150°C, once and twice.

Curves that correspond to as-deposited films are deconvoluted so that we noticed some peaks that are assigning to α and β-Si_3N_4. After the first annealing, the

curve of A_2 sample shows that some peaks have disappeared and some other have appeared to form more sharp crests and that is easily explaining by the rearrangement of atoms under the effect of the annealing. Therefore, shapes of those broad-bands are due to the formation of small-sized nanoparticles of α and β-Si_3N_4 regarding the width and the position of the known Si peak. Oxygen bounds have been also detected and disappeared after consecutive annealing probably it due to the oxidation layer caused by the exposure of the substrate after chemical treatment and before deposition process.

But, the delay of the treatment and the fixed temperature have indicated to us that these weren't sufficient to transform all structures formed to β phase even after the second annealing steps depicted for the A_3 sample. We have noticed that there is an accentuation of the phenomenon yet observed, and the formation of nanostructures has been demonstrated by the shift of the prominent peak of Si at (514 cm^{-1}). Oxygen bonds disappear under the calcination process confirmed by the attenuation of the O_2 resonance peak.

The shift towards the right, i.e the blue-shift, viewed after the first annealing process indicates the generation of the compressive stress in all samples. Thereafter, we observe a slight shift towards the left (red-shift) with the second annealing process. Residual tensile is the stresses remained in a body when all external forces have removed. These stresses [58,59] are a consequence of the annealing and also can have its origin from the inhomogeneous impact of heat over the film surface. This pattern of residual stress is presenting in all samples and is not relating to the elaboration process.

The Raman spectroscopy response linked to the as-deposited film denoted B_1 reveals that the combinations of the peaks of bounds resonance are exclusively affiliated to α-Si_3N_4. The pointed peaks corresponding to (320 nm^{-1} and 570 nm^{-1}) are sharp enough to say so that this elaboration has formed a crystallized film. After the first annealing process, the majority of peaks in B_1 have disappeared in B_2 to one major Silicon crest at 517 cm^{-1} frequency linked to the formation of nanostructures [59,60] knowing that the diamond structure of mono-crystalline silicon allows only one first-order Raman active phonon, which corresponds to the transverse optic (TO) of Si at 520.5 cm^{-1}. Besides, some smaller peaks are appeared and assigned to α-Si_3N_4 andβ-Si_3N_4 phases, which are respectively identified by the Raman shifts located at ~153, 284, 321, 563 and 608 cm^{-1} due to the Si-N-Si symmetric vibrational modes and by the

Raman shifts located at 210, 619 and 1045 cm^{-1} [61][62]. However, these peaks appear more clearly in narrow nice shapes indicating good crystallinity.

Furthermore, the Raman spectroscopy of the C and D samples have also indicated the coexistence of the both α and β phases exhibiting approximately the same vibrational modes, but only the one difference, which is linked to the particles size. In this case, particles tend to have smaller sizes, which will be explained in SEM analysis.

IV.3. Morphology of surfaces

In order to further characterize the Si_3N_4 and heat treatment effects on microstructural properties of the silicon nitride film, SEM analysis was carried out as shown in Figures IV-6, IV-7 and IV-8.

The figure IV-6 shows SEM images of Si_3N_4 for samples A_1, B_1, C_1 and D_1 as-deposited by PECVD:
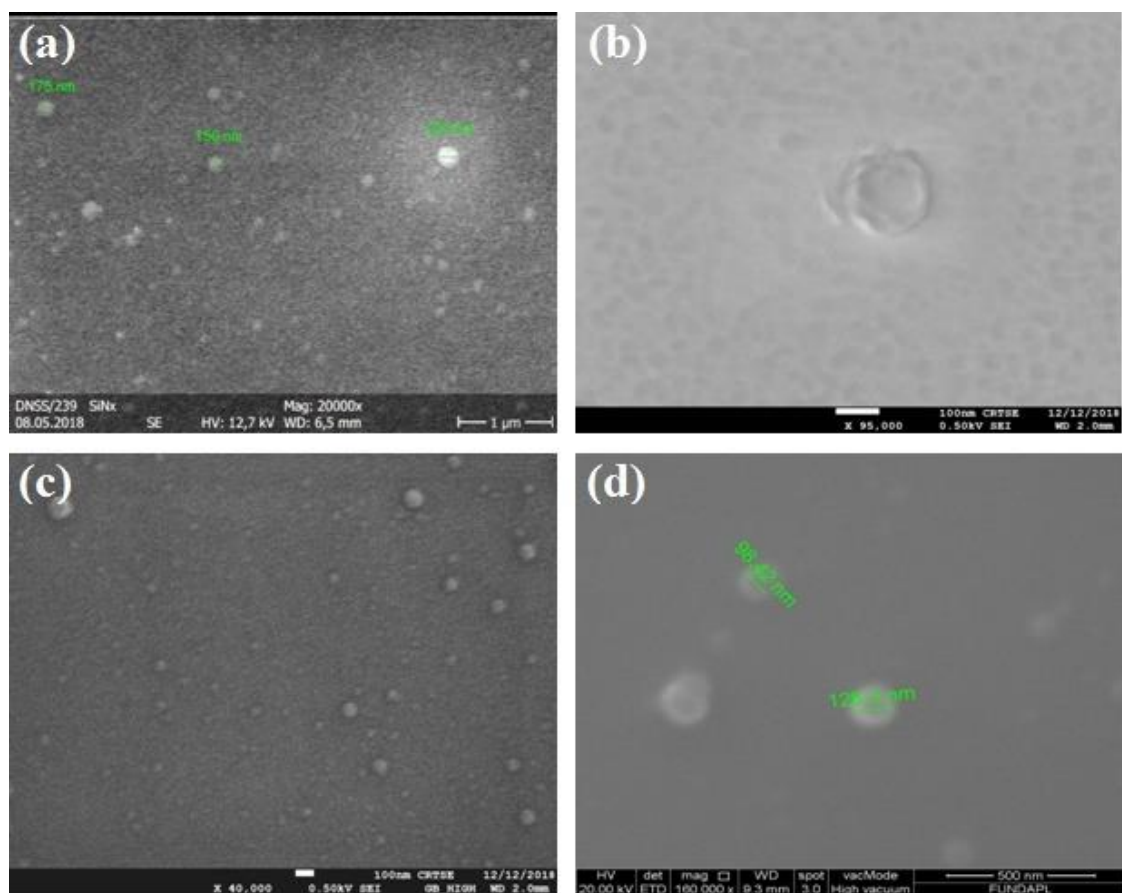
Figure IV-6: SEM images of thin layer of silicon nitride for samples all samples (a) – A_1, (b) – B_1, (c) – C_1, (d) –D_1 as deposited by PECVD.

It is noted that the morphology of the surface of a thin layer of Si_3N_4 as-deposited is fully covered, uniform and homogeneous. However, there is the beginning of the formation of nanoparticles which become quite apparent, scattered on the surface and which concentrates in agglomerates of larger size (100-220 nm) visible on the image A_1, B_1 and D_1 and we also note a defect of the deposits on the image B_1. Globally the surfaces have a rough appearance.

The figure IV-7 shows SEM images of Si_3N_4 for samples $A_{.3}$,B_3, $C_3$and D_3heated once and twice at 1150°C.
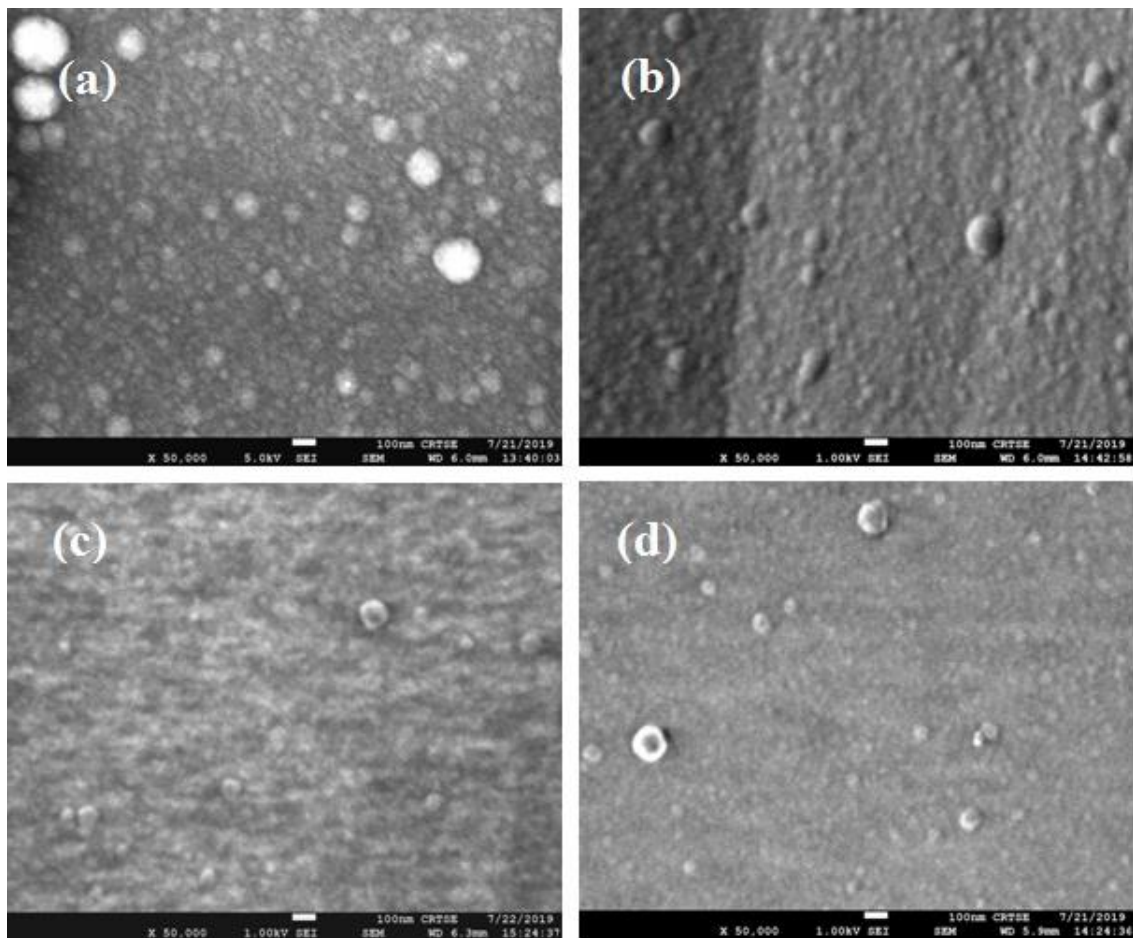
Figure IV-7: SEM images of thin layer of Si_3N_4 for samples all samples (a) - A_3, (b) - B_3, (c) - C_3, (d) - D_3 deposited by PECVD after annealing at 1150°C, once and twice.

The morphology of the layers having undergone heat treatment reveals a difference in contrast between the film bottom and the surface nanostructures. It shows that the surface of the darker bottom is dense and composed of grains, there is appearance of nanoparticles scattered on the surface of all samples.

The figure IV-8 shows SEM images of Si_3N_4 for samples A_3, B_3, C_3 and D_3 heated once and twice at 1150°C with metallization.

Due to the non-conductive properties of silicon nitride, the electron microscopy becomes hard to perform because of the saturation, in interest to avoid saturation of electron a thin layer of a conductive material needs to be deposited on the surface in order to deposit thin layer of silver, we used the thermal evaporation under vacuum to minimize the contamination of the thin layer during the deposition by nitrogen or water vapor present in the atmosphere that collides with the atoms that escapes from the vapor of the material. The result was satisfactory and the images were clear allowing as seeing clearly the presence of nanoparticles scattered on the surface of all samples.
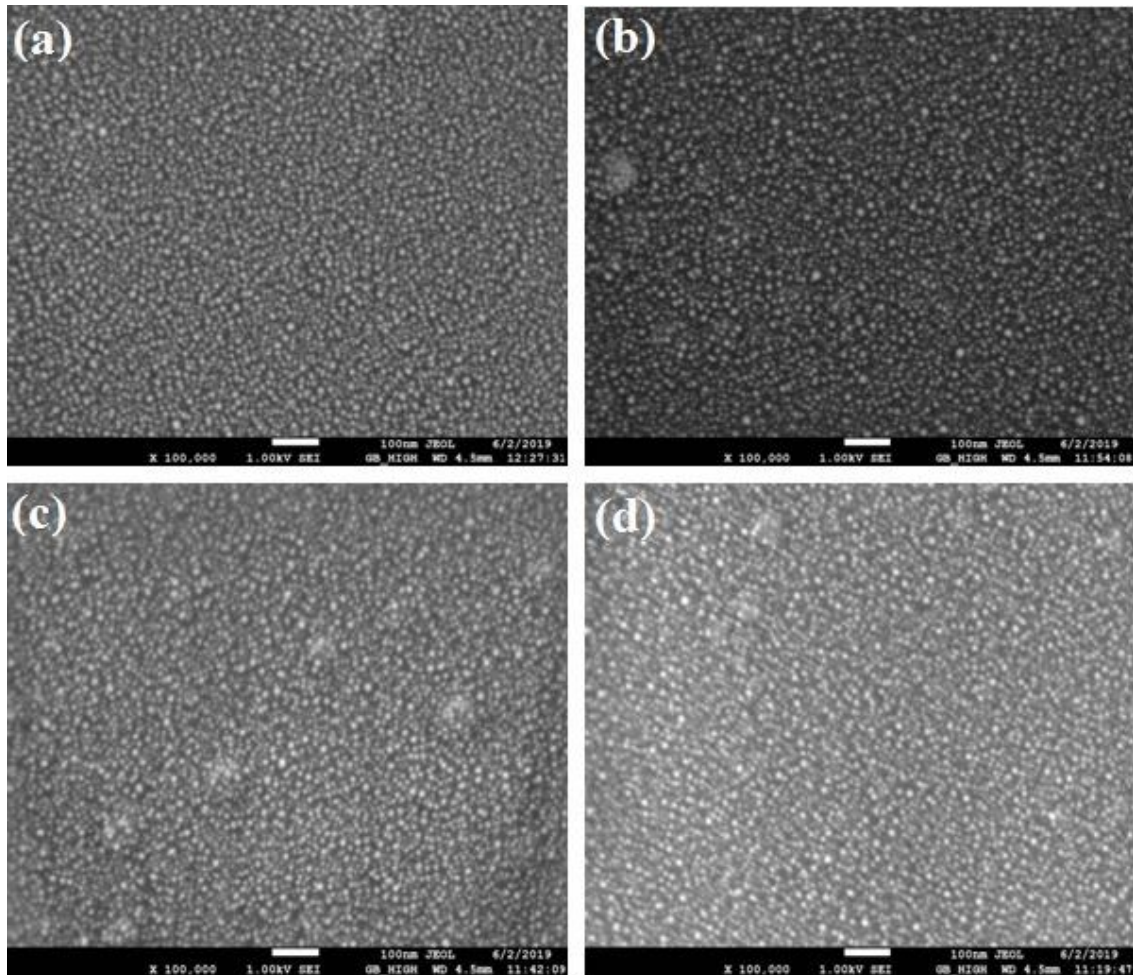
Figure IV-8: SEM images of thin layer of Si_3N_4 for samples all samples (a) - A_3, (b) - B_3, (c) - C_3, (d) - D_3 deposited by PECVD after annealing at 1150°C, once and twice with metallization.

IV.4. Surface roughness from SEM images using Image J software results

To study the surface morphology and roughness of the film, AFM images of thin layers of Si_3N_4 provided from A_3, B_3, C_3, and D_3 annealed samples has been predicted using the ImageJ software. The surface roughness is plotting from Si_3N_4 SEM micrographs of corresponding samples.

The figure IV-9 and figure IV-10 show surface roughness plot of Si_3N_4 films assigned to A_3, B_3, C_3 and D_3 samples heated at 1150°C.

Surface roughness is an important parameter in the determination of many physical properties because it is one of the information indicating the state of surface morphology and grain-size.The roughness measurements obtained on the A_3 film tends to be higher due to the formation of nanometer-sized particles [63]. As for B_3Sample, the roughness has slightly decreased. However, samples C_3 and D_3 show a change in surface morphology and roughness tends to be lower, which means that the size of nano-metric particles can be reduced to very fine particles, resulting in low roughness.
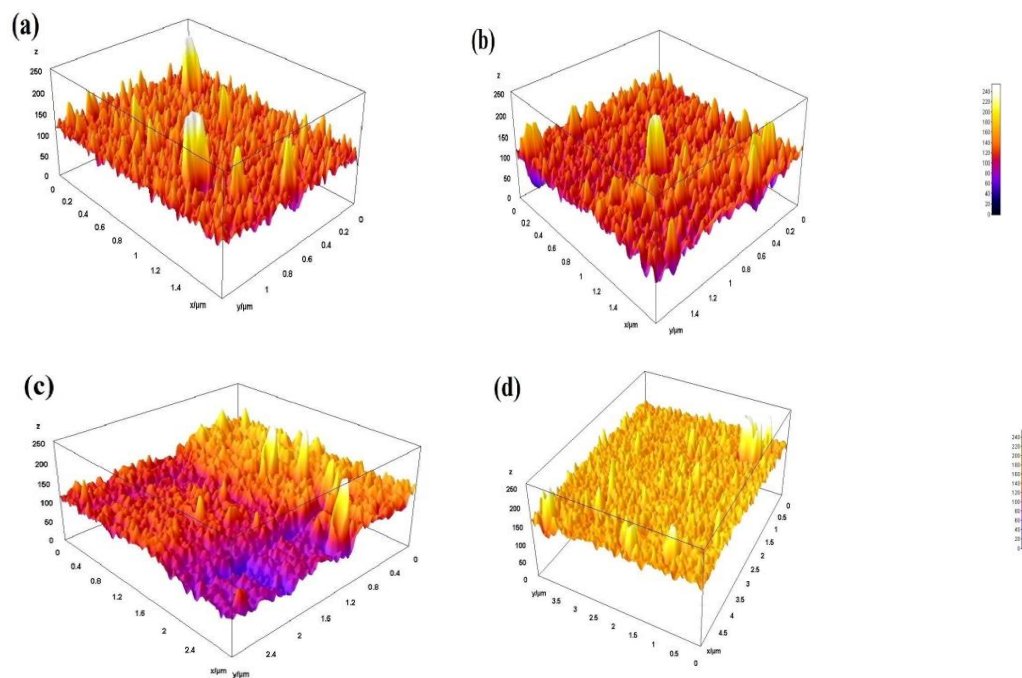
Figure IV-9: Typical AFM images prediction of surface topography of all samples (a) - A_3, (b) - B_3, (c) - C_3, (d) - D_3 using ImageJ software.
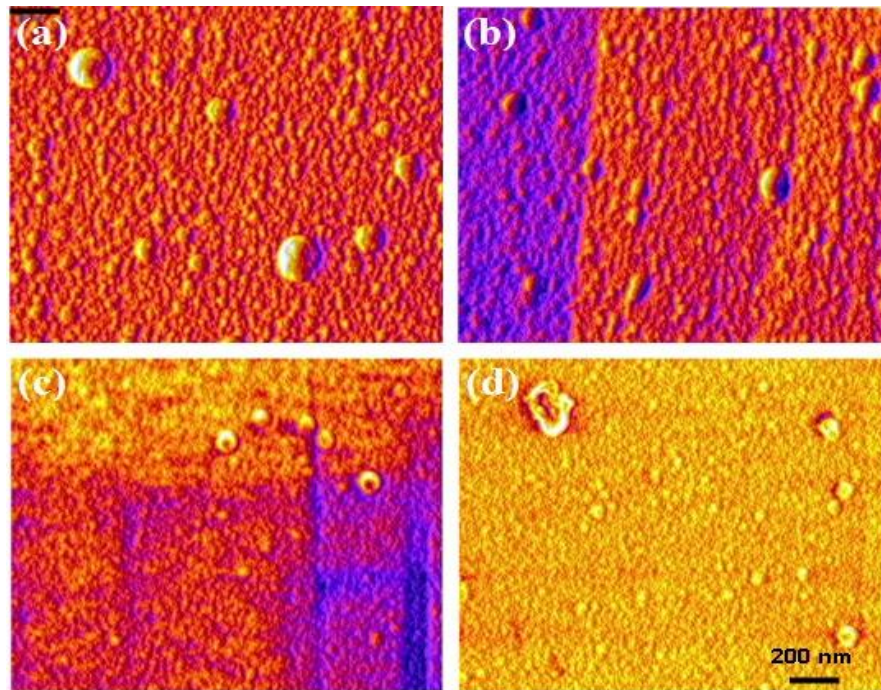
Figure IV-10: AFM images prediction of all samples (a) – A_3, (b) – B_3, (c) – C_3, (d) – D_3 using ImageJ software.

IV.5.Optical characterization

IV.5.1. Diffuse reflectance

Figure IV-11 groups all reflectance spectra of the Si_3N_4 thin films assigned to as-deposited, heated once and twice samples at 1150°C. The reflectance spectra of the Si_3N_4 thin films show us that in each sample we notice similar behavior depending on the in-situ elaboration parameters. For the sample A three peaks of absorbance are noted, for as-deposited sample denoted A_1 we have noticed peaks at 700 nm, (3 %) sharp peak at 450 nm and the last one at 350 nm. As for samples denoted A_2 and A_3, we notice a decrease of reflectance intensity and a redshift for absorbance peaks from 700 nm to 676 nm and from 450 nm to 436 nm.

For the B sample, two characteristic peaks of absorbance are noted .In the sample denoted B_1,we have noticed peaks at 800 nm and 500 nm. Thereafter applying annealing process once and twice for the samples denoted B_2 and B_3, respectively, we have also observed a decrease of reflectance intensity by 12% and a redshift for absorbance peak from 500 nm to 439 nm.

IV. Results and Discussions
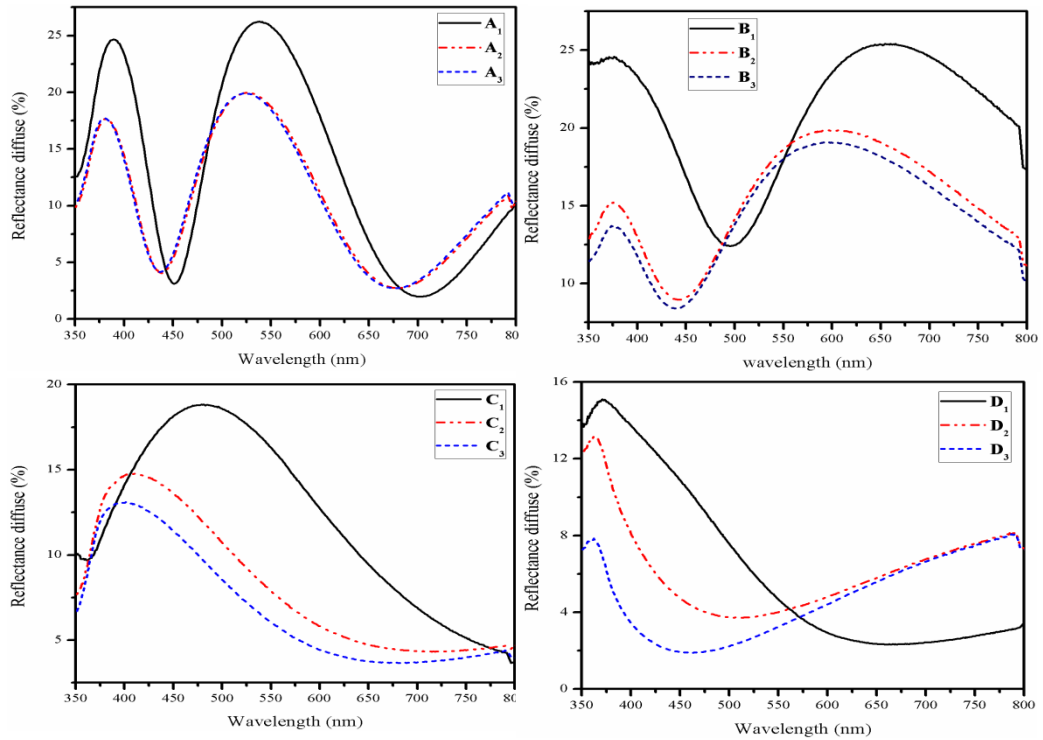
Figure IV-11: Reflectance spectra of Si_3N_4 film of all samples considering the case of as deposited and annealed at 1150°C, once and twice.

For the sample C, the as-deposited sample denoted C_1 (18.8 %) peak of reflectance is noted at 482 nm [64], as for the samples denoted C_2 and C_3 annealed at 1150°C, 1150°C we notice a decrease of reflectance intensity by 4% for sample C_2 and 6 % for the sampleC_3 and a redshift from 482 nm to 402 nm.

As for sample D the as-deposited sample denoted D_1 (15.3 %) peak of reflectance is noted at 370 nm, as for the samples denoted D_2 and D_3 annealed at 1150°C, 1150°C we notice a decrease of reflectance intensity by 1.85% for sample D_2 and 7.15 % for the sample D_3 and a small redshift from 370 nm to 362 nm.

From our results, we can conclude that deposition technique and the temperature are significant factors determining the reflectance and absorbance properties of the Si_3N_4 thin film. All samples have a low reflection in the UV-Vis range. We observe for the Si_3N_4 film that the reflection peak reaches the value of ~19.35% corresponding to 465 nm. There is one drop in reflection is found at ~375 nm in A, B and D samples, which attributed to the threshold of absorption of Si_3N_4. However, the C sample exhibits a reflectance peak at 400 nm. The reflectance extremum was moved down with the number of annealing process.

IV.5.2. The band gap energy:

The calculation of the band gap energy can be done by UV–Visible spectroscopy, using diffuse reflectance (RD) technique [65]. The function of remission of Kubelka–Munk was applied to the values obtained from reflectance spectra. Such function, denoted by F ($_\infty$) is defined as follows:

$$F (R_\infty) = \frac{(1-R_\infty)2}{2R_\infty} \qquad (1)$$

Where $R_\infty = R_{sample}/R_{standar}$. A numerical treatment is per-formed to obtain the value of the band gap energy, using the following expression:

$$[F (R_\infty) hv]^2 = C_1(hv - E_g) \qquad (2)$$

Where C_1 is the proportionality constant, hv is the energy of the incident photon and E_g is the band gap energy. By making an extension of the curve toward the value $[F(R_\infty)hv]^2=0$, it can be found the energy value of the optical band gap of the nanostructures. This process was done in all samples to determine the corresponding optical band gaps.

The intersection between the linear fit and the photon energy axis gives the value to E_g. So, by this method, the assignment of band gap can be made.

Figure IV-12 shows the values obtained once the Kubelka–Munk function was applied to the reflectance spectra of Si_3N_4 Sample A as deposited and annealed at 1150°C, once and twice.

The Kubelka-Munk spectra of the Si_3N_4 film in three cases for all samples shown below. Originally, it can show three bands gap values, which due to the Si (100) substrate [66], the formed native SiO_2 [60] and the surface impurities. Furthermore, we focus only to last one case, which present the surface layer of Silicon nitride. Three samples are considered, the as-deposited Si_3N_4, the annealed sample at 1150°C, the second annealed at the same temperature. Figure IV-12 shows the values obtained once the Kubelka–Munk function was applied to the reflectance spectra of Si_3N_4 Sample A as deposited and annealed at 1150°C, once and twice. For as-deposited film denoted A_1 it has the smallest bandgap energy, Eg (3.27eV), which corresponds to the reflectance

edge wavelength of 379.1 nm while for samples A_2 and A_3 the bandgap energy has slightly increase Eg (3.30 eV), Eg (3.31eV), respectively.
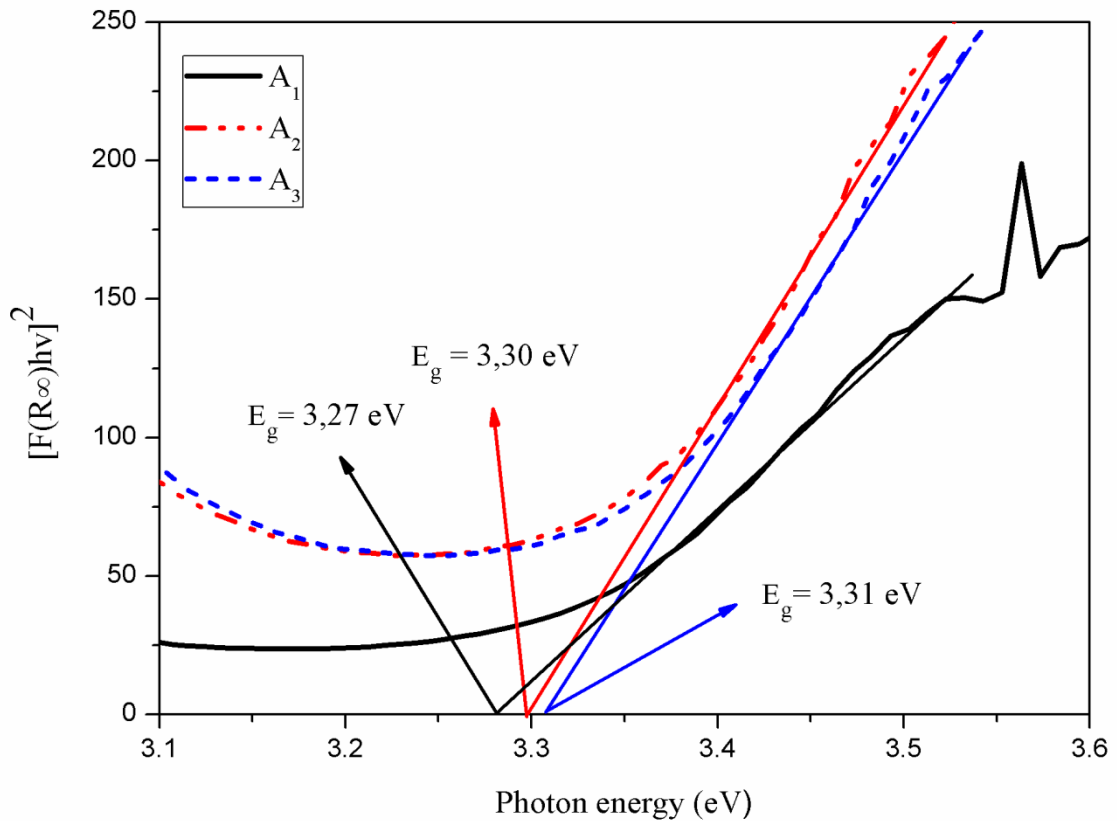
Figure IV-12: Values of Kubelka–Munk function applied to reflectance spectra of Si_3N_4 sample A as deposited and annealed at 1150°C, once and twice.

Figure IV-13 shows the values obtained once the Kubelka–Munk function was applied to the reflectance spectra of Si_3N_4 Sample B as deposited and annealed at 1150°C, once and twice.

The kubelka-munk spectra of the Si_3N_4 film in three cases for the sample B are shown in Figure IV-13 Originally it can show three bands gap values, which due to the Si (100) substrate [66], the formed native SiO_2 [60] and the surface impurities. Furthermore, we focus only to last one case, which present the surface layer of Silicon nitride. Three samples are considered, the as deposited Si_3N_4, the annealed sample at 1150°C, the second annealed at the same temperature. For as deposited film denoted B_1 it has the smallest band gap energy, Eg (3.25eV), which corresponds to the reflectance edge wavelength of 381.5 nm, while for samplesB_2 the band gap energy has increase Eg (3.32eV), corresponding to the reflectance edge wavelength of 373.4 nm. Then, the

IV. Results and Discussions

band gap energy has slightly decrease for samples B_3 Eg (3.27eV), which corresponds to the reflectance edge wavelength of 379.2 nm.
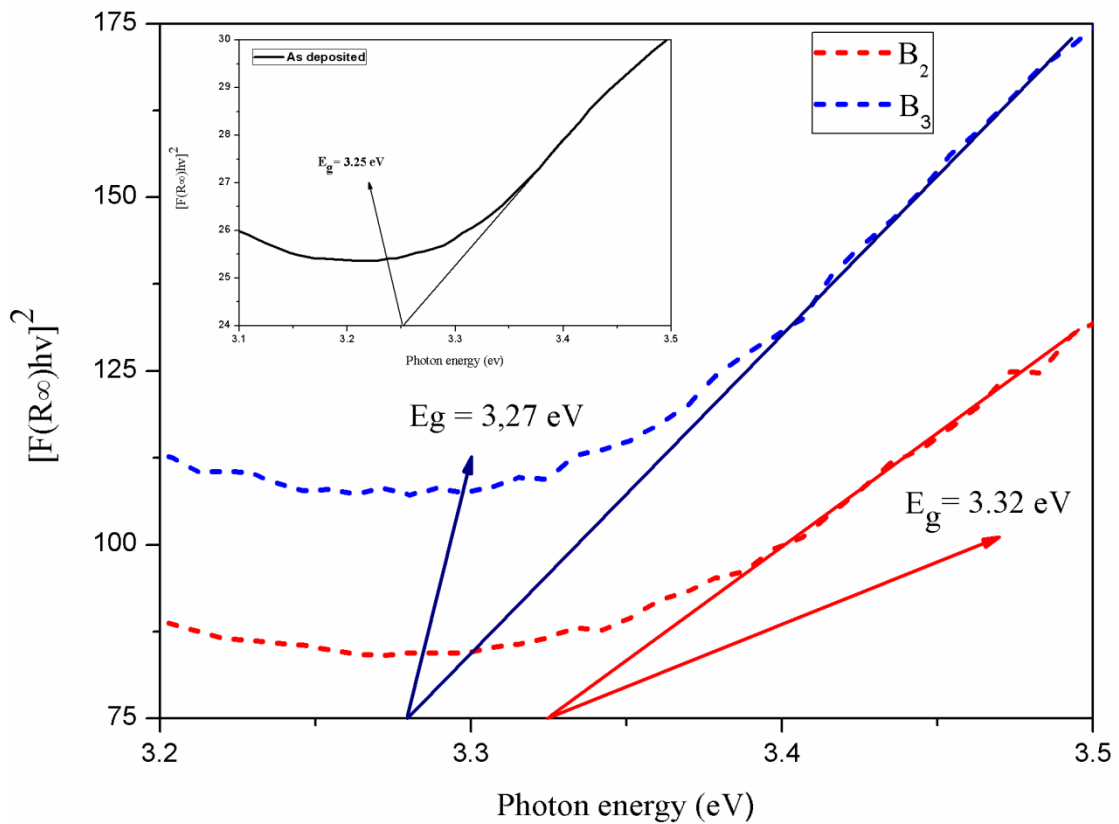
Figure IV-13: Values of Kubelka–Munk function applied to reflectance spectra of Si_3N_4 sample B as deposited and annealed at 1150°C, once and twice.

Figure IV-14 shows the values obtained once the Kubelka–Munk function was applied to the reflectance spectra of Si_3N_4 Sample C as deposited and annealed at 1150°C, once and twice.

The kubelka-munk spectra of the Si_3N_4 film in three cases for the sample C are shown in Figure IV-14 Originally it can show three bands gap values, which due to the Si (100) substrate [66], the formed native SiO_2 [60] and the surface impurities. Furthermore, we focus only to last one case, which present the surface layer of Silicon nitride. Three samples are considered, the as deposited Si_3N_4, the annealed sample at 1150°C, the second annealed at the same temperature. For as deposited film denoted C_1 it has the smallest band gap energy, Eg (3.05 eV), which corresponds to the reflectance edge wavelength of 406.5 nm while for samples C_2 and C_3 the band gap energy has

increase Eg (3.27 eV), Eg (3.32eV) respectively, which corresponds to the reflectance edge wavelength of 379.1 nm and 373.4 nm.
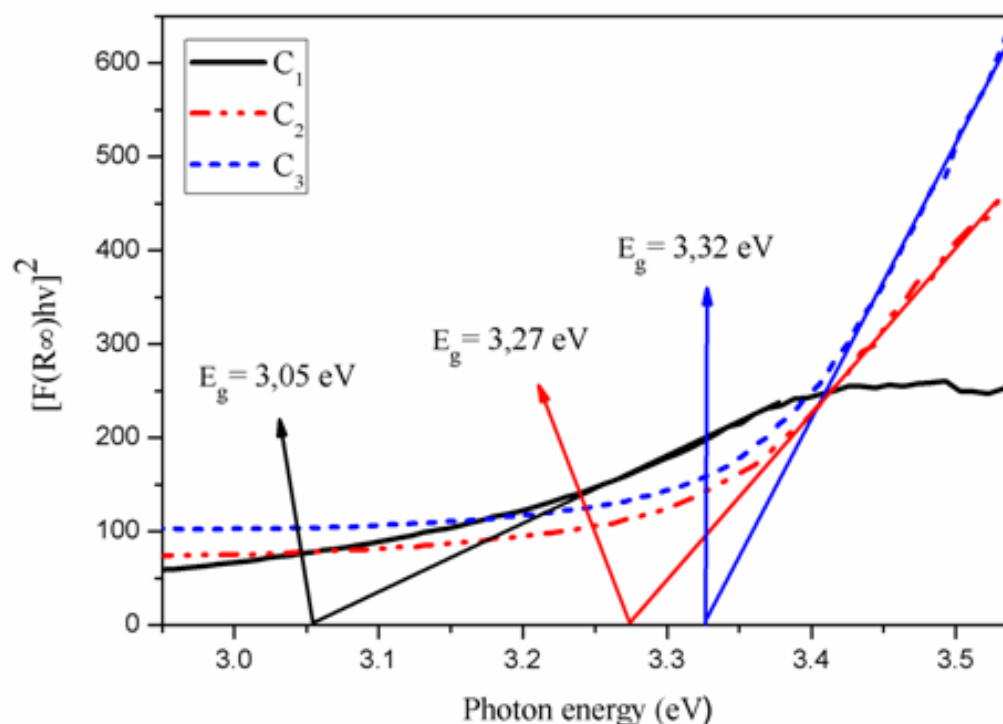
Figure IV-14: Values of Kubelka–Munk function applied to reflectance spectra of Si_3N_4 sample C as deposited and annealed at 1150°C, once and twice.

Figure IV-15 shows the values obtained once the Kubelka–Munk function was applied to the reflectance spectra of Si_3N_4 Sample D as deposited and annealed at 1150°C, once and twice.

The kubelka-munk spectra of the Si_3N_4 film in three cases for the sample D are shown in Figure IV-15 Originally it can show three bands gap values, which due to the Si (100) substrate [66], the formed native SiO_2 [60] and the surface impurities. Furthermore, we focus only to last one case, which present the surface layer of Silicon nitride. Three samples are considered, the as deposited Si_3N_4, the annealed sample at 1150°C, the second annealed at the same temperature. For as deposited film denoted D_1 it has the smallest band gap energy, Eg (3.36eV), which corresponds to the reflectance edge wavelength of 369 nm while for samples D_2 and D_3 the band gap energy has increase Eg (3.45eV), Eg (3.47 eV) respectively, which corresponds to the reflectance edge wavelength of 359.4 nm and 357.3 nm.
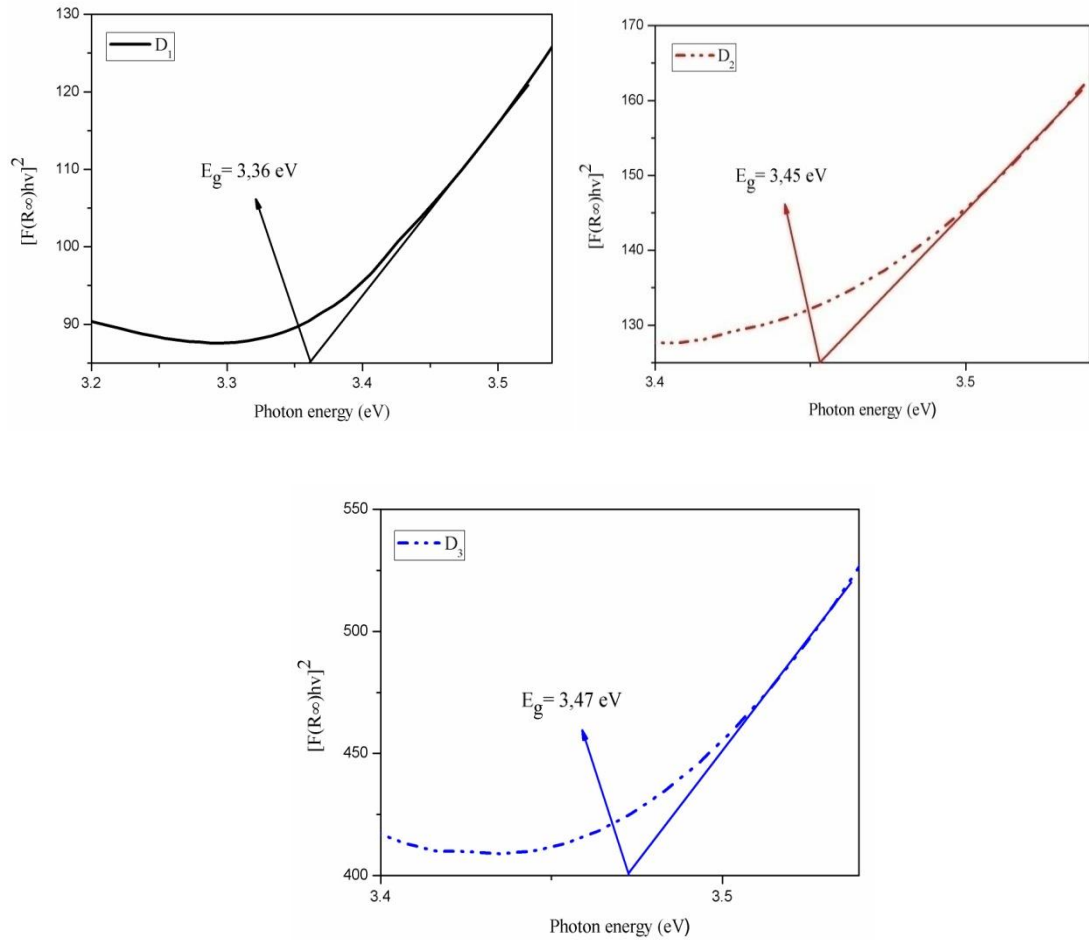
Figure IV-15: Values of Kubelka–Munk function applied to reflectance spectra of
Si₃N₄ sample D as deposited and annealed at 1150°C, once and twice.

The slight change in reflectance and bandgap energy of the three samples who have undergone a second anneal to 1150°C, can be attributed to temperature. However, other factors can affect the value of the bandgap energy, apart from the temperature, for example, the effect of size, dopants, defects, tensions, and the functionalization with organic surfactants [67].

IV.6. Lifetime results

To test the passivation properties of the films, we used (WCT-120, Sinton Instruments), Wafers used for this purpose were solar grade, p-type. The lifetime of the samples was measured via the quasi-steady-state photo conductance method (QSSPC).

The carrier lifetime tests structures of the interface between crystalline silicon and stoichiometric silicon nitride have been comprehensively studied to investigate the surface behavior.

The figure IV-16 shows measured lifetime images of Si_3N_4 for samples A_1, B_1, C_1 and D_1 as deposited by PECVD:
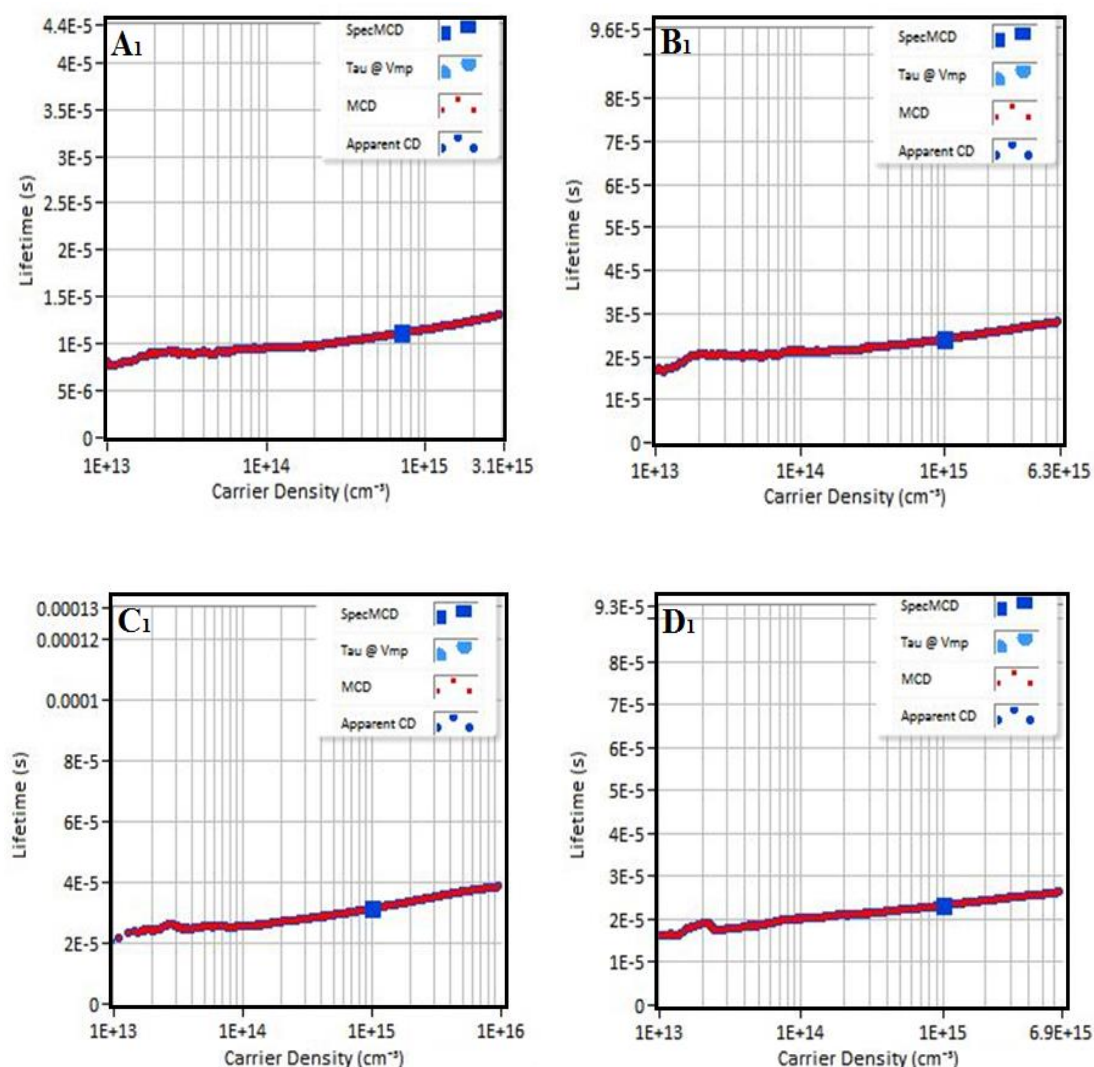
Figure IV-16: Measured lifetimes of thin layer of silicon nitride for all samples as deposited by PECVD.

Table IV-2: Details of measured lifetime in these experiments.

Samples	A_1	B_1	C_1	D_1
Lifetime at spec.MCD (µs)	11.1	24	31.28	23.28
Total sheet resistance (Ohm/sq)	34.96	32.74	42.64	32.46
Measured resistivity (Ohm.cm)	1.29	1.21	1.45	1.1
Doping (cm^{-3})	$1.06.10^{17}$	$1.06.10^{17}$	$1.06.10^{17}$	$1.06.10^{17}$
Doping type	P	P	P	P
Implied Voc (mV)	636.9	658.4	666.1	659.4
Implied FF (%)	84.34	81.77	82.28	83.38

To enhance the efficiency of a solar cell we have to coat the surface with a passivation layer to decrease its recombination rate [68]. The increased surface recombination rate leads to increased losses of the photo-generated electron-hole pairs near the surface. Even when it is high it can form a dead region where every electron-hole pairs will be killed in this region. Knowing that most of the UV photons are absorbed near the surface [69], then an appreciable portion of the incident solar spectrum will be ineffective. In the end, the photocurrent of the solar cell increases with reducing the surface recombination.

It noticed in table IV-2 the total sheet resistance differs as the lifetime, because of the elaboration condition used to elaborate the samples. However, the highest lifetime was recorded for the sample C_1 up to (31.28 µs), the decrease in lifetime concludes that the hydrogen passivation was successful.

General Conclusion

In this work, we studied the structural, morphological and optical properties of Silicon nitride (Si_3N_4) thin layers prepared by Plasma-Enhanced Chemical Vapor Deposition (PECVD). The deposition of the Si_3N_4 layers was performed on p-type silicon substrates. A systematic study of the effect of heat treatment at different steps on the properties of the deposited layers has been carried out.

The scanning electron microscopy images of Si_3N_4 thin films have demonstrated the presence of nanoparticles which have increased with annealing temperature.

The results of the XRD demonstrated the formation of hexagonal structure with the coexistence of both α and β phases. The Raman results showed that the crystalline quality depends on the elaboration conditions.

The prediction of AFM images using ImageJ software demonstrated high surface roughness, which tends to be smoothed in the case of D sample.

Optical characterization by diffuse reflectance revealed that the deposited films can be a good absorption and reflective material. The optical gap values are between 3.24 eV and 3.47 eV for all samples.

With all this properties, we have answered many questions of elaboration of a material that can be anti-reflective coating for solar cells [70]. Within the low band gap and surface morphology that it can be used in the electronics industry as a passivation layer to protect semiconductor devices [71] and as a gate dielectric layers in thin-film transistors (TFT) and an insulator layers to fabricate metal-nitride-oxide-silicon (MNOS) devices [72].

Perspective

☑ The conditions used for possible growth of β-Si_3N_4 from the α-Si_3N_4 beta phase decrease due to the applied conditions favoring the formation of the alpha phase. However, a post annealing at high temperature of 1850°C should be applied to synthesis β-Si_3N_4.

☑ The optimized silicon nitride can be as antireflective coating [73] and surface passivation layer in solar cells but the formation nano-structured particles is the challenge needed to the optoelectronics devices.

Reference

[1] X.Hu, C. Shao, J. Wang, H. Wang and J. Cheng, Effects of residual radicals on compositional and structural stability of silicon nitride fibers, J. Eur. Ceram. Soc.37 (2017) 4497–4503, https://dx.doi.org/10.1016/j.jeurceramsoc.2017.06.035.

[2] X.Hu, C. Shao and J. Wang, Surface defect healing effect of silica coatings on silicon nitride fibers, Ceram Int. 43 (2017) 16703–16709, https://dx.doi.org/ 10.1016/j.ceramint.2017.09.061.

[3] H.Klemm, Silicon Nitride for High-Temperature Applications, Journal of the American Ceramic Society. 93 (2010) 1501–1522, https://dx.doi.org/10.1111/j.1551-2916.2010.03839.x.

[4] D.Bučevac, S.Bošković, B.Matović, Kinetics of the α−β Phase Transformation in Seeded Si_3N_4 Ceramics, Science of Sintering. 40 (2008) 263–270, https://dx.doi.org/ 10.2298/SOS0803263B.

[5] J.Huang, Z.Huang , S.Yi , Y.Liu , M. Fang and S. Zhang, Fe-catalyzed growth of one-dimensional α-Si_3N_4 nanostructures and their cathode-luminescence properties, Scientific Reports . 3 (2013) 1–9, https://dx.doi.org/10.1038/srep03504.

[6] J.Huang, S.Zhang, Z.Huang, Y.Liua and M.Fanga, Growth of α-Si_3N_4nanobelts via Ni-catalyzed thermal chemical vapour deposition and their violet-blue luminescent properties, Cryst. Eng. Comm. 15 (2013) 785–790, https://dx.doi.org/10.1039/c2ce26484f.

[7] W.Yang, Z.Xie, H.Miao, L.Zhang, H.Ji and L.An, Synthesis of Single Crystalline Silicon Nitride NanobeltsViaCatalyst Assisted Pyrolysis of a Polysilazane, Journal of American Ceramic Society. 88 (2005) 457–462, https://dx.doi.org/10.1111/j.1551-2916.2005.00069.x.

[8] Y.Zhang, N.Wang, R.He, J.Liu, X.Zhang and J.Zhu, A simple method to synthesize Si_3N_4 and SiO_2 nanowires from Si or Si/SiO_2 mixture, Journal of Crystal Growth. 233 (2001) 803–808, https://dx.doi.org/10.1016/s0022-0248(01)01650-5.

[9] J.Huang, S.Zhang, Z.Huang, M. Fang, Y.Liu and K.Chen, Co-catalyzed nitridation of silicon and in-situ growth of α-Si_3N_4nanorods, Ceramics International. 40 (2014) 11063-11070, https://dx.doi.org/10.1016/j.ceramint.2014.03.1.2.

[10] A.Stass, P.Bieringer, W.Hansch, V.Fuenzalida, A.Alvarez, J.luna, I.Martil, F.L. Martinez and I.Eisele, Fabrication and characterization of thin low-temperature MEB-compatible silicon oxides of different stoichiometry, Thin Solid Films. 349 (1999) 135-146, https://dx.doi.org/10.1016/s0040-6090(99)00166-2.

[11] K.L.Choy, Chemical vapour deposition of coatings, Progress in Materials Science. 48 (2003) 57-170, https://dx.doi.org/10.1016/s0079-6425 (01)00009-3.

[12] A.Shih, S.Yeh, S.Lee and T.R.Yang, Structural differences between deuterated and hydrogenated silicon nitride/oxynitride, Journal of Applied Physics. 89 (2001) 5355-5361, https://dx.doi.org/10.1063/1.1364645.

Reference

[13] R.C.Sangster and D.J.Fisher, Si_3N_4 products, uses and markets, Silicon Nitride from 19th to 21st Century, 2nd ed. Geneva, Switzerland. 2015.

[14] J.F. Lelievre, Elaboration de SiN_x:H par PECVD: optimization des proprieties optique, passivantes et structurales pour applications photovoltaiques, L'institut National des sciences Appliquées de Lyon, (Doctoral Thesis). 2007.

[15] P.Pradhan, Growth and Characterizations of Silicon nitride thin films on Silicon substrates, National Institute of Technology, Rourkela Rourkela – 769008, Odisha, India. (Master Thesis). 2013.

[16] I.Guler, Optical and structural characterization of silicon nitride thin films deposited by PECVD, Materials Science and Engineering B. 246 (2019) 21-26, https://dx.doi.org/10.1016/j.mseb.2019.05.024.

[17] J.W.Mellor, A Comprehensive Treatise on Inorganic and Theoretical Chemistery, London, New York, Longmans, Green. 1 (1947), https://dx.doi.org/10.1002/jctb.5000434804.

[18] F.L.Riley, Silicon Nitride and Related Materials, Journal of the American Ceramic Society. 83 (2000) 245-265, https://dx.doi.org/10.1111/j.1151-2916.2000.tb01182.x.

[19] Y.Nishi, R.Doering, Handbook of Semiconductor Manufacturing Technology, CRC Press.(2007), https://dx.doi.org/10.1201/9781420017663.

[20] D. Hardie and K. H. Jack, Crystal Structures of Silicon Nitride, Nature. 180 (1957) 332–333, https://dx.doi.org/10.1038/180332a0.

[21] J.Z. Jiang, F. Kragh, D. J. Frost, K. Ståhl and H. Lindelov, Hardness and thermal stability of cubic silicon nitride, Journal of Physics: Condensed Matter. 13 (2001) 515-520, https://dx.doi.org/10.1088/0953-8984/13/22/111.

[22] X.Zhu, Y.Sakka,Textured silicon nitride: processing and anisotropic properties, Science and Technology of Advanced Materials. 9 (2008) 1-47, https://dx.doi.org/10.1088/1468-6996/9/3/033001.

[23] V.K.Sarin, On the α-to-β phase transformation in silicon nitride, Materials Science and Engineering. 105 (1988) 151-159, https://dx.doi.org/10.1016/0025-5416(88)90491-0.

[24] D.T.Spencer, J.F.Bauters, M.J.R.Heckand J.E.Bowers, Integrated waveguide coupled Si_3N_4 resonators in the ultrahigh-Q regime, Optica. 3 (2014) 153–157, https://dx.doi.org/10.1364/optica.1.000153.

[25] J.F.Bauters, M.J.R.Heck, D.D.John, J.S.Barton, C.M.Bruinink, A.Leinse, R.G.Heideman, D.J.Blumenthal and J.E.Bowers, Planar waveguides with less than 0.1dB/m propagation loss fabricated with wafer bonding, Optics Express. 24 (2011) 24090–24101, https://dx.doi.org/10.1364/oe.19.024090.

[26] Purnawirman, J.Sun, T.N.Adam, G.Leake, D.Coolbaugh, J.D.B.Bradley, E.S.Hosseini and M.R.Watts, CandL-banderbium-doped waveguide lasers with wafer Scale silicon nitride cavities, Opt Lett. 11 (2013) 1760–1763, https://dx.doi.org/10.1364/ol.38.001760.

Reference

[27] W.D.Sacher, Z.Yong, J.C.Mikkelsen, A.Bois, Y.Yang, J. C. Mak, P. Dumais, D. Goodwill, C.Ma, J.Jeong, E.Bernier and J.K.Poon, Multilayer silicon nitride-on-silicon integrated photonic platform for 3D photonic circuits, Conference on Lasers and Electro-Optics.3 (2016).

[28] A.Z.Subramanian, P.Neutens, A.Dhakal, R.Jansen, T.Claes, X.Rottenberg, F.Peyskens, S.Selvaraja, P.Helin, B.DuBois, K.Leyssens, S.Severi, P.Deshpande, R.Baets and P.V.Dorpe, Low-losssing lemode PECVD silicon nitride photonic wire waveguides for 532-900 nm wavelength window fabricated within a CMOS pilot line, IEEE Photonics J. 6 (2013) 2202809–2202809. https://dx.doi.org/10.1109/jphot.2013.2292698.

[29] S.R.Garcia, F.Merget, F.Zhong, H.Finkelstein and J.Witzens, Silicon nitride CMOS-compatible platform for integrated photonics applications at visible wavelengths, Optics Express. 12 (2013) 14036–14046. https://dx.doi.org/10.1364/oe.21.014036.

[30] R.Heiderman, M.Hoekman and E.Schreuder, TriPle Xbased integrated optical ring resonators for lab-on-a-chip and environmental detection, IEEEJ Quantum Electron. 5 (2012) 1583–1596. https://dx.doi.org/10.1109/jstqe.2012.2188382.

[31] L.Moressi, Basics of Molecular Beam Epitaxy (MBE) technique, Bentham Science Publishers. (2013) 81-107, https://dx.doi.org/10.2174/97816080551801130101.

[32] G.Kovačević and B.Pivac, Reactions in silicon–nitrogen plasma, Physical Chemistry Chemical Physics. 19 (2017) 3826–3836, https://dx.doi.org/10.1039/c6cp05395e.

[33] A.Dollet, J.P.Couderc and B.Despax, Analysis and numerical modelling of silicon nitride deposition in a plasma-enhanced chemical vapour deposition reactor, part I: Bidimensional modeling, Plasma Sources Science and Technology. 4 (1995) 94-106, https://dx.doi.org/10.1088/0963-0252/4/1/010.

[34] H.J. Yuan, S. Xie, D.F.Liu, X.Q.Yan, Z.P.Zhou, L.J.Ci, J.X.Wang, Y.Gao, L.Song, L.F.Liu, W.Y.Zhou, G.Wang, Characterization of zinc oxide crystal nanowires grown by thermal evaporation of ZnS powders, Chemical Physics Letters. 4 (2003) 337–341. https://dx.doi.org /0.1016/s0009-2614(03)00293-8.

[35] W.Yang, Z.Xie, J Li, H.Miao, L.Zhang and L.An, Ultra-Long Single-Crystalline alpha-Si_3N_4 Nanowires: Derived from a Polymeric Precursor, Journal of the American Ceramic Society. 88 (2005) 1647–1650, https://dx.doi.org /0.1111/j.1551-2916.2005.00270.x.

[36] S.Liu, M. Fang, Z.Huang, J.Huang, H.Ji , H.Liu, Y.Liu and X.Wu1, $Fe(NO_3)_3$-assisted large-scale synthesis of Si_3N_4 nanobelts from quartz and graphite by carbo thermal reduction–nitridation and their photoluminescence properties, Scientific Reports. 5 (2015), https://dx.doi.org/10.1038/srep08998.

[37] N.Sun, X.Meng and Z.Xiaon, Functionalized Si_3N_4 nanoparticles modified with hydrophobic polymer chains by surface-initiated atom transfer radical polymerization (ATRP), Ceramics International. 41 (2015) 13830–13835, https://dx.doi.org/10.1016/j.ceramint.2015.08.068.

Reference

[38] P.M.Martin, Handbook of Deposition Technologies for Films and Coatings. (2010) 1–31. https://dx.doi.org/10.1016/b978-0-8155-2031-3.00001-6.

[39] F.K Shan and Y. S. Yu, Band gap energy of pure and Al-doped ZnO thin films, Journal of the European Ceramic Society. 24 (2004) 1869-1872. https://dx.doi.org/10.1016/s0955-2219(03)00490-4.

[40] A.Zerga, Caractérisation, Modélisation et Simulation Numérique des Cellules Photovoltaïques à base de Silicium Polycristallin en Couche Mince Déposée par RTCVD, (Doctoral Thesis), université de Tlemcen. 2005.

[41] M.K.Esfahani, Application of SiGe(C) in high performance MOSFETs and infrared detectors, KTH, School of Information and Communication Technology (ICT), (Doctoral Thesis). 2011.

[42] H.F.Sterling and R.C.G.Swann, Chemical vapour deposition promoted by r.f. radio-frequency discharge, Solid-State Electronics. 8 (1965) 653-654, https://dx.doi.org/10.1016/0038-1101(65)90033-x.

[43] R.Hezel and R.Schorner, Plasma Si nitride—A promising dielectric to achieve high-quality silicon MIS/IL solar cells, Journal of Applied Physics. 52 (1981) 3076–3079. https://dx.doi.org/10.1063/1.329058.

[44] A.GAberle. Overview on SiN Surface Passivation of crystalline silicon solar cells.Solar Energy Materials and Solar Cells. 1 (2001) 239-248. https://dx.doi.org/10.1016/s0927-0248(00)00099-4.

[45] A.G.Aberle, T.L.auinger and R.Hezel, Comparison of Direct and Remote PECVD Silicon Nitride Films for Low-Temperature Surface Passivation of P-Type Crystalline Silicon,H.S. Stephens and Associates. 1 (1997).

[46] S.Eränen and A.Inoue, Handbook of Silicon Based MEMS Materials and Technologies. (Second Edition) 2015.

[47] J.A.lazar, R.L.Estopier, E.Q.González, A.M.Sánchez, J.P.Chávez, I.E.Z.Huerta and M.A.Mijares, Silicon-Rich Oxide Obtained by Low-Pressure Chemical Vapor Deposition to Develop Silicon Light Sources, Chemical Vapor Deposition - Recent Advances and Applications in Optical, Solar Cells and Solid State Devices. (2016) 160-180, https://dx.doi.org/10.5772/63012.

[48] T.Otani, M.Hirata,High rate deposition of silicon nitride films by APCVD, Thin Solid Films. 442 (2003) 44-47, https://dx.doi.org/10.1016/S0040-6090(03)00938-6.

[49] Chrisey, D.B.Hubler, G.KHubler, Pulsed Laser Deposition of Thin Films, NJ, USA, 1994.

[50] R.Eason, Pulsed Laser Deposition of Thin Films–Applications-Led Growth of Functional Materials, Wiley-Interscience: Hoboken, NJ, USA. 2006 1–682.

Reference

[51] H.Kim, T.E.Sutto and A.Piqué, Laser materials processing for micropower source applications: a review, Journal of Photonics for Energy. 4 (2014) 1-21, https://dx.doi.org/10.1117/1.jpe.4.040992.

[52] D.J. Gardiner, P.R. Graves,Practical Raman Spectroscopy,Springer-VerlagBerlin Heidelberg. (1989), https://dx.doi.org/10.1007/978-3-642-74040-4.

[53] Petres, Roman, Amorphous Silicon Compound Films for Surface Passivation and Antireflection Coating of Crystalline Silicon Solar Cells, Konstanz: University of Konstanz.(Dissertation) (2010).

[54] S. Liu, M. Fang, Z. Huang, J. Huang, H.Ji, H.Liu, Y.Liu and X.Wu, $Fe(NO_3)^3$ assisted large-scale synthesis of Si_3N_4 nanobelts from quartz and graphite by carbo thermal reduction–nitridation and their photoluminescence properties. 5 (2015) 1-8, https://dx.doi.org/10.1038/srep08998.

[55] Z.Tatl, F.Çalışkan, J.Butler, C.Crowley and S. Hampshire, SPS sintering of silicon nitride with fluoride additive. Ceramics International. 40 (2014) 1399–1404. https://dx.doi.org/10.1016/j.ceramint.2013.07.021.

[56] A.C.Lee, H.Lu, T.H.Lin, P.Šajgalík, F.D.Lii, P.K.Nayak, J.L.Huang, Nanopowder processing of ultrafine Si_3N_4 with improved wear resistance. Journal of Asian Ceramic Societies. 3(2015) 6–12. https://dx.doi.org/10.1016/j.jascer.2014.09.004.

[57] N.Wada, S.A.Solin, J.Wong and S.Prochazka, Raman and IR absorption specroscopic studies on α, β and amorphous Si_3N_4, Journal of Non-Crystalline Solids. 43 (1980) 7-15, https://dx.doi.org/10.1016/0022-3093(81)90169-1.

[58] Ch.Ossadnik, S.Veprek and I.Gregora, Applicability of Raman scattering for the characterization of nanocrystalline silicon.Thin Solid Films. 337 (1999) 148-151, https://dx.doi.org/10.1016/S0040-6090(98)01175-4.

[59] S. Veprek, F.A. Sarottand Z. Iqbal, Effect of grain boundaries on the Raman spectra, optical absorption, and elastic light scattering in nanometer-sized crystalline silicon. Phys Rev. 36 (1987) 3344-3350, https://dx.doi.org/10.1103/PhysRevB.36.3344.

[60] Y.Tao, J.Zheng, Y.Zuo, C.Xue, B Cheng, Qiming Wang Enhanced Current Transportation in Siliconriched Nitride (SRN)/Silicon-riched Oxide (SRO) Multilayer Nanostructure Nano-Micro Lett. 4 (2012) 202-207, https://dx.doi.org/10.3786/nml.v4i4.p202-207.

[61] U.Degenhardt, F.Stegner, C.Liebscher, U.Glatzel, K.Berroth, W.Krenkel and Motz. Sintered silicon nitride/nano-silicon carbide materials based on preceramic polymers and ceramic powder. Journal of the European Ceramic Society. 32 (2012) 1893–1899, https://dx.doi.org/10.1016/j.jeurceramsoc.2011.09.007.

[62] N.Muraki, G.Katahiri, V.Sergo, G.Pezzotti, T.Nishida, Mapping of residual stresses around an indentation in β-Si3N4 using Raman spectroscopy. J Mater Sci. 32 (1997) 19–23, https://dx.doi.org/10.1023/a:1018639516582.

Reference

[63] T.Grigaitis, A.Naujokaitis , S.Tumėnas , G.Juška and K.Arlauskas, Characterization of silicon nitride layers deposited in three-electrode plasma-enhanced CVD chamber. Lithuanian Journal of Physics. 55 (2015) 35–43, https://dx.doi.org/10.3952/physics.v55i1.3056.

[64] K.Jhansirani, R.S Dubey, M.A.More, S.Singh, Deposition of Silicon Nitride Films using Chemical Vapor deposition for Photovoltaic Applications, Results in Physics. 6 (2016) 1059-1063, https://dx.doi.org/10.1016/j.rinp.2016.11.029.

[65] A.E.Morales, E.S.Mora, U.Pal, Use of diffuse reflectance spectroscopy for optical characterization of un-supported nanostructures, Revista Mexicana De F´isica. 3 (2007) p18-22.

[66] T.V.Torchynska, J.L.Casas Espinola, E.V.Hernandez, L.Khomenkova, F.Delachat and A. Slaoui, Effect of the stoichiometry of Si-rich silicon nitride thin films on their photoluminescence and structural properties. Thin Solid Films. 581(2015) 65–69, https://dx.doi.org/10.1016/j.tsf.2014.11.070.

[67] V.Muşat, A.Tăbăcaru, B.Vasile, V.A.Surdu, Size-dependent photoluminescence of zinc oxide quantum dots through organo silane functionalization. RSC Adv. 108 (2014) 63128-63136, https://dx.doi.org/10.1039/c4ra10851e.

[68] T.Jana, S.Mukhopadhyay, S.Ray , Low temperature silicon oxide and nitride for surface passivation of silicon solar cells, Solar Energy Materials and Solar Cells. 71 (2002) 197–211, https://dx.doi.org/10.1016/s0927-0248(01)00058-7.

[69] Muñoz, E.Monroy, E.Pau, J.L.Calle, F.Omnès and P.Gibart, III nitrides and UV detection. Journal of Physics. 13 (2001) 7115–7137, https://dx.doi.org/10.1088/0953-8984/13/32/316.

[70] Sharma and Rajinder, Silicon nitride as antireflection coating to enhance the conversion efficiency of silicon solar cells, Turkish Journal of Physics. 42 (2018) 350-355, https://dx.doi.org/10.3906/fiz-1801-28.

[71] R.S.Bonilla, B.Hoex, P.Hamer and P.R.Wilshaw, Dielectric surface passivation for silicon solar cells. Phys Status Solidi A. 7 (2017), https://dx.doi.org/10.1002/pssa.201700293.

[72] A.Dhakal, F.Peyskens , S.Clemmen , A.Raza, P.Wuytens, H.Zhao, Le Thomas N, Baets R. Single mode waveguide platform for spontaneous and surface-enhanced on-chip Raman spectroscopy. Interface Focus. 6 (2016), https://dx.doi.org/10.1098/rsfs.2016.0015.

[73] Y.Tao, J.Zheng, Y.Zuo, C. Xue, B.Cheng, Q.Wang. Enhanced Current Transportation in Silicon-riched Nitride (SRN)/Silicon-riched Oxide (SRO) Multilayer Nanostructure. Nano-Micro Lett. 4 (2012) 202-207, https://dx.doi.org/10.3786/nml.v4i4.p202-207.